Total Variation in Imaging

V. Caselles
DTIC, Universitat Pompeu-Fabra,
C/Roc Boronat 138, 08018, Barcelona, Spain
e-mail: vicent.caselles@upf.edu

A. Chambolle
CNRS UMR 7641, Ecole Polytechnique
91128 Palaiseau Cedex, France
e-mail: antonin.chambolle@polytechnique.fr

M. Novaga
Dipartimento di Matematica, Università di Padova
via Trieste 63, 35121 Padova, Italy
e-mail: novaga@math.unipd.itt

Abstract

The use of total variation as a regularization term in imaging problems was motivated by its ability to recover the image discontinuities. This is at the basis of his numerous applications to denoising, optical flow, stereo imaging and 3D surface reconstruction, segmentation, or interpolation, to mention some of them. On one hand, we review here the main theoretical arguments that have been given to support this idea. On the other, we review the main numerical approaches to solve different models where total variation appears. We describe both the main iterative schemes and the global optimization methods based on the use of max-flow algorithms. Then we review the use of anisotropic total variation models to solve different geometric problems and its use in finding a convex formulation of some non convex total variation problems. Finally we study the total variation formulation of image restoration.

1 Introduction

The Total Variation model in image processing was introduced in the context of image restoration [57] and image segmentation, related to the study of the Mumford-Shah segmentation functional [34]. Being more related to our purposes here, let us consider the case of image denoising and restoration.

We assume that the degradation of the image occurs during image acquisition and can be modeled by a linear and translation invariant blur and additive noise:

$$f = h * u + n, \tag{1}$$

where $u : \mathbb{R}^2 \to \mathbb{R}$ denotes the ideal undistorted image, $h : \mathbb{R}^2 \to \mathbb{R}$ is a blurring kernel, f is the observed image which is represented as a function $f : \mathbb{R}^2 \to \mathbb{R}$, and n is an additive white noise with zero mean and standard deviation σ. In practice, the noise can be considered as Gaussian.

A particular and important case contained in the above formulation is the denoising problem which corresponds to the case where $h = \delta$, so that equation (1) is written as

$$f = u + n, \tag{2}$$

where n is an additive Gaussian white noise of zero mean and variance σ^2.

The problem of recovering u from f is ill-posed. Several methods have been proposed to recover u. Most of them can be classified as regularization methods which may take into account statistical properties (Wiener filters), information theoretic properties [36], a priori geometric models [57] or the functional analytic behaviour of the image given in terms of its wavelet coefficients (see [50] and references therein).

The typical strategy to solve this ill-conditioning is regularization [58]. In the linear case the solution of (1) is estimated by minimizing a functional

$$J_\gamma(u) = \| Hu - f \|_2^2 + \gamma \| Qu \|_2^2, \tag{3}$$

which yields the estimate

$$u_\gamma = (H^t H + \gamma Q^t Q)^{-1} H^t f, \tag{4}$$

where $Hu = h * u$, and Q is a regularization operator. Observe that to obtain u_γ we have to solve a system of linear equations. The role of Q is, on one hand, to move the small eigenvalues of H away from zero while leaving the large eigenvalues unchanged, and, on the other hand, to incorporate the a priori (smoothness) knowledge that we have on u.

If we treat u and n as random vectors and we select $\gamma = 1$ and $Q = R_s^{-1/2} R_n^{1/2}$ with R_s and R_n the image and noise covariance matrices, then (4) corresponds to the Wiener filter that minimizes the mean square error between the original and restored images.

One of the first regularization methods consisted in choosing between all possible solutions of (1) the one which minimized the Sobolev (semi) norm of u

$$\int_{\mathbb{R}^2} |Du|^2 \, dx, \tag{5}$$

which corresponds to the case $Qu = Du$. In the Fourier domain the solution of (3) given by (4) is $\hat{u} = \frac{\overline{\hat{h}}}{|\hat{h}|^2 + 4\gamma\pi^2|\xi|^2} \hat{f}$. From the above formula we see that high frequencies of f (hence, the noise) are attenuated by the smoothness constraint.

This formulation was an important step, but the results were not satisfactory, mainly due to the inability of the previous functional to resolve discontinuities (edges) and oscillatory textured patterns. The smoothness required by the finiteness of the Dirichlet integral (5) constraint is too restrictive. Indeed, functions in $W^{1,2}(\mathbb{R}^2)$ (i.e., functions $u \in L^2(\mathbb{R}^2)$ such that $Du \in L^2(\mathbb{R}^2)$) cannot have discontinuities along rectifiable curves. These observations

motivated the introduction of Total Variation in image restoration problems by L. Rudin, S. Osher and E. Fatemi in their work [57]. The a priori hypothesis is that functions of bounded variation (the BV model) [10] are a reasonable functional model for many problems in image processing, in particular, for restoration problems [57]. Typically, functions of bounded variation have discontinuities along rectifiable curves, being continuous in some sense (in the measure theoretic sense) away from discontinuities [10]. The discontinuities could be identified with edges. The ability of total variation regularization to recover edges is one of the main features which advocates for the use of this model but its ability to describe textures is less clear, even if some textures can be recovered, up to a certain scale of oscillation. An interesting experimental discussion of the adequacy of the BV-model to describe real images can be found in [42].

In order to work with images, we assume that they are defined in a bounded domain $\Omega \subseteq \mathbb{R}^2$ which we assume to be the interval $[0, N[^2$. As in most of the works, in order to simplify this problem, we shall assume that the functions h and u are periodic of period N in each direction. That amounts to neglecting some boundary effects. Therefore, we shall assume that h, u are functions defined in Ω and, to fix ideas, we assume that $h, u \in L^2(\Omega)$. Our problem is to recover as much as possible of u, from our knowledge of the blurring kernel h, the statistics of the noise n, and the observed image f.

On the basis of the BV model, Rudin-Osher-Fatemi [57] proposed to solve the following constrained minimization problem

$$\begin{aligned} &\text{Minimize} \quad \int_\Omega |Du| \\ &\text{subject to} \quad \int_\Omega |h * u(x) - f(x)|^2 \, dx \leq \sigma^2 |\Omega|. \end{aligned} \tag{6}$$

Notice that the image acquisition model (1) is only incorporated through a global constraint. Assuming that $h * 1 = 1$ (energy preservation), the additional constraint that $\int_\Omega h * u \, dx = \int_\Omega f(x)$ is automatically satisfied by its minima [24]. In practice, the above problem is solved via the following unconstrained minimization problem

$$\text{Minimize} \int_\Omega |Du| + \frac{1}{2\lambda} \int_\Omega |h * u - f|^2 \, dx \tag{7}$$

where the parameter λ is positive. Recall that we may interpret λ as a penalization parameter which controls the trade-off between the goodness of fit of the constraint and the smoothness term given by the Total Variation. In this formulation, a methodology is required for a correct choice of λ. The connections between (6) and (7) were studied by A. Chambolle and P.L. Lions in [24] where they proved that both problems are equivalent for some positive value of the Lagrange multiplier λ.

In the denoising case, the unconstrained variational formulation (7) with $h = \delta$ is

$$\text{Minimize} \int_\Omega |Du| + \frac{1}{2\lambda} \int_\Omega |u - f|^2 \, dx, \tag{8}$$

and it has been the object of much theoretical and numerical research (see [11, 58] for a survey). Even if this model represented a theoretical and practical progress in the denoising

problem due to the introduction of BV functions as image models, the experimental analysis readily showed its main drawbacks. Between them, let us mention the staircasing effect (when denoising a smooth ramp plus noise, the staircase is an admissible result), the pixelization of the image at smooth regions and the loss of fine textured regions, to mention some of them. This can be summarized with the simple observation that the residuals $f-u$, where u represents the solution of (8), do not look like noise. This has motivated the development on non local filters [17] for denoising, the use of a stochastic optimization techniques to estimate u [49], or the consideration of the image acquisition model as a set of local constraints [3, 4] to be discussed below.

Let us finally mention that, following the analysis of Y. Meyer in [50], the solution u of (8) permits to obtain a decomposition of the data f as a sum of two components $u+v$ where u contains the geometric sketch of f while v is supposed to contain its noise and textured parts. As Meyer observed, the L^2 norm of the residual $v := f-u$ in (8) is not the right one to obtain a decomposition of f in terms of geometry plus texture and he proposed to measure the size of the textured part v in terms of a dual BV norm showing that some models of texture have indeed a small dual BV norm.

In spite of its limitations, the Total Variation model has become one of the basic image models and has been adapted to many tasks: optical flow, stereo imaging and 3D surface reconstruction, segmentation, interpolation, or the study of $u + v$ models to mention a few cases. On the other hand, when compared to other robust regularization terms, it combines simplicity and geometric character and makes it possible a rigorous analysis. The theoretical analysis of the behavior of solutions of (8) has been the object of several works [6, 14, 15, 52, 50, 20] and will be summarized in Sections 3 and 4.

Recall that one of the main reasons to introduce the Total Variation as a regularization term in imaging problems was its ability to recover discontinuities in the solution. This intuition has been confirmed by the experimental evidence and has been the motivation for the study of the local regularity properties of (8) in [20, 21]. After recalling in Section 2 some basic notions and results in the theory of bounded variation functions, we prove in Section 3.1 that the set of jumps (in the BV sense) of the solution of (8) is contained in the set of jumps of the datum f [20]. In other words, model (8) does not create any new discontinuity besides the existing ones. As a refinement of the above statement, the local Hölder regularity of the solutions of (8) is studied in Section 3.2. This has to be combined with results describing which discontinuities are preserved. No general statement in this sense exists but many examples are described in the papers [11, 14, 15, 7]. The preservation of a jump discontinuity depends on the curvature of the level line at the given point, the size of the jump and the regularization parameter λ. This is illustrated in the example given in Section 4. The examples support the idea that total variation is not perfect but may be a reasonable regularization term in order to restore discontinuities.

Being considered as a basic model, the numerical analysis of the total variation model has been the object of intensive research. Many numerical approaches have been proposed in order to give fast, efficient methods which are also versatile to cover the whole range of applications. In Section 5 we review some basic iterative methods introduced to solve the

Euler-Lagrange equations of (8). In particular, we review in Section 5.2 the dual approach introduced by A. Chambolle in [25]. In Section 5.3 we review the primal dual scheme of Zhu and Chan [60]. Both of them are between the most popular schemes by now. In Section 6 we discuss global optimization methods based on graph-cut techniques adapted to solve a quantized version of (8). Those methods have also become very popular due to its efficiency and versatility in applications and are an active area of research, as it can be seen in the references. Then, in Section 7.1 we review the applications of anisotropic TV problems to find the global solution of geometric problems. Similar anisotropic TV formulations appear as convexifications of nonlinear energies for disparity computation in stereo imaging, or related problems [29, 54], and they are reviewed in Section 7.2.

In Section 8 we review the application of Total Variation in image restoration (6), describing the approach where the image acquisition model is introduced as a set of local constraints [3, 4, 56].

We could not close this Chapter without reviewing in Section 9 a recent algorithm introduced by C. Louchet and L. Moisan [49] which uses a Bayesian approach leading to an estimate of u as the expected value of the posterior distribution of u given the data f. This estimate requires to compute an integral in a high dimensional space and the authors use a Monte-Carlo method with Markov Chain (MCMC) [49]. In this context, the minimization of the discrete version of (8) corresponds to a Maximum a Posterior (MAP) estimate of u.

2 Notation and preliminaries on BV functions

2.1 Definition and basic properties

Let Ω be an open subset of $\mathbb{R}^N$. Let $u \in L^1_{\text{loc}}(\Omega)$. Recall that the distributional gradient of u is defined by

$$\int_\Omega \sigma \cdot Du = -\int_\Omega u(x) \text{div}\, \sigma(x)\, dx \, \forall C_c^\infty(\Omega, \mathbb{R}^N),$$

where $C_c^\infty(\Omega; \mathbb{R}^N)$ denotes the vector fields with values in $\mathbb{R}^N$ which are infinitely differentiable and have compact support in Ω. The total variation of u in Ω is defined by

$$V(u, \Omega) := \sup \left\{ \int_\Omega u \ \text{div}\, \sigma \ dx : \sigma \in C_c^\infty(\Omega; \mathbb{R}^N), |\sigma(x)| \leq 1 \ \forall x \in \Omega \right\}, \tag{9}$$

where for a vector $v = (v_1, \ldots, v_N) \in \mathbb{R}^N$ we set $|v|^2 := \sum_{i=1}^N v_i^2$. Following the usual notation, we will denote $V(u, \Omega)$ by $|Du|(\Omega)$ or by $\int_\Omega |Du|$.

Definition 2.1. *Let $u \in L^1(\Omega)$. We say that u is a function of bounded variation in Ω if $V(u, \Omega) < \infty$. The vector space of functions of bounded variation in Ω will be denoted by $BV(\Omega)$.*

Using Riesz representation Theorem [10], the above definition can be rephrased by saying that u is a function of bounded variation in Ω if the gradient Du in the sense of distributions is a (vector valued) Radon measure with finite total variation $V(u, \Omega)$.

Recall that $BV(\Omega)$ is a Banach space when endowed with the norm $\|u\| := \int_\Omega |u|\, dx + |Du|(\Omega)$. Recall also that the map $u \to |Du|(\Omega)$ is $L^1_{\rm loc}(\Omega)$-lower semicontinuous, as a sup (9) of continuous linear forms [10].

2.2 Sets of finite perimeter. The coarea formula

Definition 2.2. *A measurable set $E \subseteq \Omega$ is said to be of finite perimeter in Ω if $\chi_E \in BV(\Omega)$. The perimeter of E in Ω is defined as $P(E,\Omega) := |D\chi_E|(\Omega)$. If $\Omega = \mathbb{R}^N$, we denote the perimeter of E in $\mathbb{R}^N$ by $P(E)$.*

The following inequality holds for any two sets $A, B \subseteq \Omega$:

$$P(A \cup B, \Omega) + P(A \cap B, \Omega) \leq P(A, \Omega) + P(B, \Omega). \tag{10}$$

Theorem 1. *Let $u \in BV(\Omega)$. Then for a.e. $t \in \mathbb{R}$ the set $\{u > t\}$ is of finite perimeter in Ω and one has*

$$\int_\Omega |Du| = \int_{-\infty}^{\infty} P(\{u > t\}, \Omega)\, dt.$$

In other words, the total variation of u amounts to the sum of the perimeters of its upper level sets.

An analogous formula with the lower level sets is also true. For a proof we refer to [10].

2.3 The structure of the derivative of a BV function

Let us denote by $\mathcal{L}^N$ and $\mathcal{H}^{N-1}$, respectively, the N-dimensional Lebesgue measure and the $(N-1)$-dimensional Hausdorff measure in $\mathbb{R}^N$ (see [10] for precise definitions). of

Let $u \in [L^1_{\rm loc}(\Omega)]^m$ $(m \geq 1)$. We say that u has an approximate limit at $x \in \Omega$ if there exists $\xi \in \mathbb{R}^m$ such that

$$\lim_{\rho \downarrow 0} \frac{1}{|B(x,\rho)|} \int_{B(x,\rho)} |u(y) - \xi| dy = 0. \tag{11}$$

The set of points where this does not hold is called the approximate discontinuity set of u, and is denoted by S_u. Using Lebesgue's differentiation theorem, one can show that the approximate limit ξ exists at $\mathcal{L}^N$-a.e. $x \in \Omega$, and is equal to $u(x)$: in particular, $|S_u| = 0$. If $x \in \Omega \setminus S_u$, the vector ξ is uniquely determined by (11) and we denote it by $\tilde{u}(x)$.

We say that u is approximately continuous at x if $x \notin S_u$ and $\tilde{u}(x) = u(x)$, that is if x is a Lebesgue point of u (with respect to the Lebesgue measure).

Let $u \in [L^1_{\rm loc}(\Omega)]^m$ and $x \in \Omega \setminus S_u$; we say that u is approximately differentiable at x if there exists an $m \times N$ matrix L such that

$$\lim_{\rho \downarrow 0} \frac{1}{|B(x,\rho)|} \int_{B(x,\rho)} \frac{|u(y) - \tilde{u}(x) - L(y-x)|}{\rho}\, dy \;=\; 0. \tag{12}$$

In that case, the matrix L is uniquely determined by (12) and is called the a approximate differential of u at x.

For $u \in BV(\Omega)$, the gradient Du is a N-dimensional Radon measure that decomposes into its absolutely continuous and singular parts $Du = D^a u + D^s u$. Then $D^a u = \nabla u \, dx$ where ∇u is the Radon-Nikodym derivative of the measure Du with respect to the Lebesgue measure in $\mathbb{R}^N$. The function u is approximately differentiable $\mathcal{L}^N$-a.e. in Ω and the approximate differential coincides with $\nabla u(x)$ $\mathcal{L}^N$-a.e. The singular part $D^s u$ can be also split in two parts: the *jump* part $D^j u$ and the *Cantor* part $D^c u$.

We say that $x \in \Omega$ is an *approximate jump point of* u if there exist $u^+(x) \neq u^-(x) \in \mathbb{R}$ and $|\nu_u(x)| = 1$ such that

$$\lim_{\rho \downarrow 0} \frac{1}{|B_\rho^+(x, \nu_u(x))|} \int_{B_\rho^+(x,\nu_u(x))} |u(y) - u^+(x)| \, dy = 0$$

$$\lim_{\rho \downarrow 0} \frac{1}{|B_\rho^-(x, \nu_u(x))|} \int_{B_\rho^-(x,\nu_u(x))} |u(y) - u^-(x)| \, dy = 0,$$

where $B_\rho^+(x, \nu_u(x)) = \{y \in B(x,\rho) \, : \, \langle y - x, \nu_u(x) \rangle > 0\}$ and $B_\rho^-(x, \nu_u(x)) = \{y \in B(x,\rho) \, : \, \langle y - x, \nu_u(x) \rangle < 0\}$. We denote by J_u the set of approximate jump points of u. If $u \in BV(\Omega)$, the set S_u is countably $\mathcal{H}^{N-1}$ rectifiable, J_u is a Borel subset of S_u and $\mathcal{H}^{N-1}(S_u \setminus J_u) = 0$ [10]. In particular, we have that $\mathcal{H}^{N-1}$-a.e. $x \in \Omega$ is either a point of approximate continuity of $\tilde{u}$, or a jump point with two limits in the above sense. Finally, we have

$$D^j u = D^s u \llcorner_{J_u} = (u^+ - u^-) \nu_u \mathcal{H}^{N-1} \llcorner_{J_u} \quad \text{and} \quad D^c u = D^s u \llcorner_{(\Omega \setminus S_u)}.$$

For a comprehensive treatment of functions of bounded variation we refer to [10].

3 The regularity of solutions of the TV denoising problem

3.1 The discontinuities of solutions of the TV denoising problem

Given a function $f \in L^2(\Omega)$ and $\lambda > 0$ we consider the minimum problem

$$\min_{u \in BV(\Omega)} \int_\Omega |Du| + \frac{1}{2\lambda} \int_\Omega (u - f)^2 \, dx \, . \tag{13}$$

Notice that problem (13) always admits a unique solution u_λ, since the energy functional is strictly convex.

As we mentioned in the Introduction, one of the main reasons to introduce the Total Variation as a regularization term in imaging problems was its ability to recover the discontinuities in the solution. This Section together with Sections 3.2 and 4 is devoted to analyze this assertion. In this Section we prove that the set of jumps of u_λ (in the BV sense) is contained in the set of jumps of f, whenever f has bounded variation. Thus, model (13) does not create any new discontinuity besides the existing ones. Section 3.2 is devoted to review a local Hölder regularity result of [21]: the local Hölder regularity of the data is inherited by the solution. This has to be combined with results describing which discontinuities are preserved. In Section 4 we give an example of explicit solution of (13) which shows that the preservation of a jump discontinuity depends on the curvature of the level line at the given

point, the size of the jump and the regularization parameter λ. Other examples are given in the papers [11, 14, 15, 7, 2]. The examples support the idea that total variation may be a reasonable regularization term in order to restore discontinuities.

Let us recall the following observation, which is proved in [26, 7, 19].

Proposition 3.1. *Let u_λ be the (unique) solution of (13). Then, for any $t \in \mathbb{R}$, $\{u_\lambda > t\}$ (respectively, $\{u_\lambda \geq t\}$) is the minimal (resp., maximal) solution of the minimal surface problem*

$$\min_{E \subseteq \Omega} P(E, \Omega) + \frac{1}{\lambda} \int_E (t - f(x))\, dx \tag{14}$$

(whose solution is defined in the class of finite-perimeter sets, hence, up to a Lebesgue-negligible set). In particular, for all $t \in \mathbb{R}$ but a countable set, $\{u_\lambda = t\}$ has zero measure and the solution of (14) is unique up to a negligible set.

A proof that $\{u_\lambda > t\}$ and $\{u_\lambda \geq t\}$ both solve (14) is found in [26, Prop. 2.2]. A complete proof of this proposition, which we do not give here, follows from the co-area formula, which shows that, up to a renormalization, for any $u \in BV(\Omega) \cap L^2(\Omega)$,

$$\int_\Omega |Du| + \frac{1}{2\lambda} \int_\Omega (u - f)^2\, dx = \int_{\mathbb{R}} \left(P\left(\{u > t\}, \Omega\right) + \frac{1}{\lambda} \int_{\{u>t\}} (t - f)\, dx \right) dt\,,$$

and from the following comparison result for solutions of (14) which is proved in [7, Lemma 4]:

Lemma 3.2. *Let $f, g \in L^1(\Omega)$ and E and F be respectively minimizers of*

$$\min_E P(E, \Omega) - \int_E f(x)\, dx \quad \text{and} \quad \min_F P(F, \Omega) - \int_F g(x)\, dx\,.$$

Then, if $f < g$ a.e., $|E \setminus F| = 0$ (in other words, $E \subseteq F$ up to a negligible set).

Proof. Observe that we have

$$P(E, \Omega) - \int_E f(x)\, dx \leq P(E \cap F, \Omega) - \int_{E \cap F} f(x)\, dx$$

$$P(F, \Omega) - \int_F g(x)\, dx \leq P(E \cup F, \Omega) - \int_{E \cup F} g(x)\, dx.$$

Adding both inequalities and using that for two sets of finite perimeter we have (10) $P(E \cap F, \Omega) + P(E \cup F, \Omega) \leq P(E, \Omega) + P(F, \Omega)$, we obtain that

$$\int_{E \setminus F} (g(x) - f(x))\, dx \leq 0.$$

Since $g(x) - f(x) > 0$ a.e., this implies that $E \setminus F$ is a null set. □

The proof of this last lemma is easily generalized to other situations (Dirichlet boundary conditions, anisotropic and/or nonlocal perimeters, see [7] and also [2] for a similar general statement). Eventually, we mention that the result of Proposition 3.1 remains true if the term $(u(x) - f(x))^2/(2\lambda)$ in (13) is replaced with a term of the form $\Psi(x, u(x))$, with Ψ of

class C^1 and strictly convex in the second variable, and replacing $(t-f(x))/\lambda$ with $\partial_u \Psi(x,t)$ in (14).

From Proposition 3.1 and the regularity theory for surfaces of prescribed curvature (see for instance [9]), we obtain the following regularity result (see also [2]).

Corollary 3.3. *Let $f \in L^p(\Omega)$, with $p > N$. Then, for all $t \in \mathbb{R}$ the super-level set $E_t := \{u_\lambda > t\}$ (respectively, $\{u_\lambda \geq t\}$) has boundary of class $C^{1,\alpha}$, for all $\alpha < (p-N)/p$, out of a closed singular set Σ of Hausdorff dimension at most $N-8$. Moreover, if $p = \infty$, the boundary of E_t is of class $W^{2,q}$ out of Σ, for all $q < \infty$, and is of class $C^{1,1}$ if $N = 2$.*

We now show that the jump set of u_λ is always contained in the jump set of f. Before stating this result let us recall two simple Lemmas.

Lemma 3.4. *Let U be an open set in $\mathbb{R}^N$ and $v \in W^{2,p}(U)$, $p \geq 1$. We have that*

$$\operatorname{div}\left(\frac{\nabla v}{\sqrt{1+|\nabla v|^2}}\right)(y) = \operatorname{Trace}\left(A(\nabla v(y)) D^2 v(y)\right) \qquad \text{a.e. in } U,$$

where $A(\xi) = \frac{1}{(1+|\xi|^2)^{\frac{1}{2}}}\left(\delta_{ij} - \frac{\xi_i \xi_j}{(1+|\xi|^2)}\right)_{i,j=1}^N$, $\xi \in \mathbb{R}^N$.

The proof follows simply by taking $\varphi \in C_0^\infty(U)$, integrating by parts in U, and regularizing v with a smoothing kernel.

Lemma 3.5. *Let U be an open set in $\mathbb{R}^N$ and $v \in W^{2,1}(U)$. Assume that u has a minimum at $y_0 \in U$ and*

$$\lim_{\rho \to 0+} \frac{1}{B_\rho(y_0)} \int_{B_\rho(y_0)} \frac{|u(y) - u(y_0) - \nabla u(y_0)\cdot(y-y_0) - \frac{1}{2}\langle D^2 v(y_0)(y-y_0), y-y_0\rangle|}{\rho^2}\, dy = 0. \tag{15}$$

Then $D^2 v(y_0) \geq 0$.

If A is a symmetric matrix and we write $A \geq 0$ (respectively, $A \leq 0$) we mean that A is positive (resp., negative) semidefinite.

The result follows by proving that $\mathcal{H}^{N-1}$-a.e. for ξ in S^{N-1} (the unit sphere in $\mathbb{R}^N$) we have $\langle D^2 v(y_0)\xi, \xi\rangle \geq 0$.

Recall that if $v \in W^{2,1}(U)$, then (15) holds a.e. on U [61, Theorem 3.4.2].

Theorem 2. *Let $f \in BV(\Omega) \cap L^\infty(\Omega)$. Then, for all $\lambda > 0$,*

$$J_{u_\lambda} \subseteq J_f \tag{16}$$

(up to a set of zero $\mathcal{H}^{N-1}$-measure).

Before giving the proof let us explain its main idea which is quite simple. Notice that, by (14), formally the Euler-Lagrange equation satisfied by ∂E_t is

$$\kappa_{E_t} + \frac{1}{\lambda}(t-f) = 0 \qquad \text{on } \partial E_t,$$

where κ_{E_t} is the sum of the principal curvatures at the points of ∂E_t. Thus if $x \in J_{u_\lambda} \setminus J_f$, then we may find two values $t_1 < t_2$ such that $x \in \partial E_{t_1} \cap \partial E_{t_2} \setminus J_f$. Notice that $E_{t_2} \subseteq E_{t_1}$ and the boundaries of both sets have a contact at x. Of the two, the smallest level set is the highest and has smaller mean curvature. This contradicts its contact at x.

Proof. Let us first recall some consequences of Corollary 3.3. Let $E_t := \{u_\lambda > t\}$, $t \in \mathbb{R}$, and let Σ_t be its singular set given by Corollary 3.3. Since $f \in L^\infty(\Omega)$, around each point $x \in \partial E_t \setminus \Sigma_t$, $t \in \mathbb{R}$, ∂E_t is locally the graph of a function in $W^{2,p}$ for all $p \in [1, \infty)$ (hence $C^{1,\alpha}$ for any $\alpha \in (0,1)$). Moreover, if $\mathcal{N} := \bigcup_{t\in\mathbb{Q}} \Sigma_t$, then $\mathcal{H}^{N-1}(\mathcal{N}) = 0$.

Let us prove that $\mathcal{H}^{N-1}(J_{u_\lambda} \setminus J_f) = 0$. Observe that we may write [10]

$$J_{u_\lambda} = \bigcup_{t_1,t_\in\mathbb{Q},t_1<t_2} \partial E_{t_1} \cap \partial E_{t_2}.$$

Thus it suffices to prove that for all $t_1, t_2 \in \mathbb{Q}$, $t_1 < t_2$, we have

$$\mathcal{H}^{N-1}\left(\partial E_{t_1} \cap \partial E_{t_2} \setminus (\mathcal{N} \cup J_f)\right) = 0. \tag{17}$$

Let us denote by B'_R the ball of radius $R > 0$ in $\mathbb{R}^{N-1}$ centered at 0. Let $C_R := B'_R \times (-R, R)$. Let us fix $t_1, t_2 \in \mathbb{Q}$, $t_1 < t_2$. Given $x \in \partial E_{t_1} \cap \partial E_{t_2} \setminus \mathcal{N}$, by Corollary 3.3, we know that there is some $R > 0$ such that, after a change of coordinates that aligns the x_N-axis with the normal to $\partial E_{t_1} \cap \partial E_{t_2}$ at x, we may write the set $\partial E_{t_i} \cap C_R$ as the graph of a function $v_i \in W^{2,p}(B'_R)$, $\forall p \in [1, \infty)$, $x = (0, v_i(0)) \in C_R \subseteq \Omega$, $\nabla v_i(0) = 0$, $i \in \{1, 2\}$. Without loss of generality, we assume that $v_i > 0$ in B'_R, and that E_{t_i} is the supergraph of v_i, $i = 1, 2$. From $t_1 < t_2$ and Lemma 3.2, it follows $E_{t_2} \subseteq E_{t_1}$, which gives in turn $v_2 \geq v_1$ in B'_R.

Notice that, since ∂E_{t_i} is of finite $\mathcal{H}^{N-1}$ measure, we may cover $\partial E_{t_1} \cap \partial E_{t_2} \setminus \mathcal{N}$ by a countable set of such cylinders. Thus, it suffices to prove that

$$\mathcal{H}^{N-1}\left((\partial E_{t_1} \cap \partial E_{t_2} \cap C_R) \setminus (\mathcal{N} \cup J_f)\right) = 0. \tag{18}$$

holds for any such cylinder C_R as constructed in the last paragraph.

Let us denote the points $x \in C_R$ as $x = (y, z) \in B'_R \times (-R, R)$. Then (18) will follow if we prove that

$$\mathcal{H}^{N-1}(\mathcal{M}_R) = 0, \tag{19}$$

where

$$\mathcal{M}_R := \{y \in B'_R : v_1(y) = v_2(y)\} \setminus \{y \in B'_R : (y, v_1(y)) \in J_f\}.$$

Recall that, by Theorem 3.108 in [10], $\mathcal{H}^{N-1}$-a.e. in $y \in B'_R$, the function $f(y, \cdot) \in BV((-R, R))$ and the jumps of $f(y, \cdot)$ are the points z such that $(y, z) \in J_f$. Recall that v_i is a local minimizer of

$$\min_v \mathcal{E}_i(v) := \int_{B'_R} \sqrt{1 + |\nabla v|^2}\, dy - \frac{1}{\lambda} \int_{B'_R} \int_0^{v(y)} (t_i - f(y, z))\, dz\, dy.$$

By taking a positive smooth test function $\psi(y)$ of compact support in B'_R, and computing $\lim_{\epsilon\to 0+} \frac{1}{\epsilon} \left(\mathcal{E}_i(v + \epsilon\psi) - \mathcal{E}_i(v)\right) \geq 0$, we deduce that

$$\operatorname{div} \frac{\nabla v_i(y)}{\sqrt{1 + |\nabla v_i(y)|^2}} + \frac{1}{\lambda} \left(t_i - f(y, v_i(y) + 0\right) \leq 0, \qquad \mathcal{H}^{N-1}\text{-a.e. in } B'_R. \tag{20}$$

In a similar way, we have

$$\operatorname{div}\frac{\nabla v_i(y)}{\sqrt{1+|\nabla v_i(y)|^2}}+\frac{1}{\lambda}\left(t_i-f(y,v_i(y)-0)\geq 0,\qquad \mathcal{H}^{N-1}\text{-a.e. in } B'_R.\right. \tag{21}$$

Finally we observe that since $v_1, v_2 \in W^{2,p}(B'_R)$ for any $p \in [1,\infty)$ and $v_2 \geq v_1$ in B'_R, by Lemma 3.5 we have that $D^2(v_1 - v_2)(y) \leq 0$ $\mathcal{H}^{N-1}$-a.e. on $\{y \in B'_R : v_1(y) = v_2(y)\}$.

Thus, if $\mathcal{H}^{N-1}(\mathcal{M}_R) > 0$, then there is a point $\bar{y} \in \mathcal{M}_R$ such that $\nabla v_1(\bar{y}) = \nabla v_2(\bar{y})$, $D^2(v_1 - v_2)(\bar{y}) \leq 0$, $f(\bar{y}, \cdot)$ is continuous at $v_1(\bar{y}) = v_2(\bar{y})$, and both equations (20) and (21) hold at $\bar{y}$. As a consequence, using Lemma 3.4 and subtracting the two equations, we obtain

$$0 \geq \operatorname{trace}(A(\nabla v_1(\bar{y}))D^2 v_1(\bar{y})) - \operatorname{trace}(A(\nabla v_2(\bar{y}))D^2 v_2(\bar{y})) = \frac{t_2 - t_1}{\lambda} > 0,$$

This contradiction proves (19). □

3.2 Hölder regularity results

Let us review the local regularity result proved in [21]: if the datum f is locally Hölder continuous with exponent $\beta \in [0,1]$ in some region $\Omega' \subset \Omega$, then a local minimizer u of (13) is also locally Hölder continuous in Ω' with the same exponent.

Recall that a function $u \in BV(\Omega)$ is a local minimizer of (13) if for any $v \in BV(\Omega)$ such that $u - v$ has support in a compact subset $K \subset \Omega$, we have

$$\int_K |Du| + \frac{1}{2}\int_K |u(x) - f(x)|^2\,dx \;\leq\; \int_K |Dv| + \frac{1}{2}\int_K |v(x) - f(x)|^2\,dx \tag{22}$$

It follows that u satisfies the equation [19]

$$-\operatorname{div} z + u \;=\; f \tag{23}$$

with $z \in L^\infty(\Omega, \mathbb{R}^N)$ with $\|z\|_\infty \leq 1$, and $z \cdot Du = |Du|$ [11].

As in Section 3.1 [20], the analysis of the regularity of the local minimizers of u is based on the following observation: for any $t \in \mathbb{R}$, the level sets $\{u > t\}$ (resp., $\{u \geq t\}$) are solutions (the minimal and maximal, indeed) of the prescribed curvature problem (14) which is defined in the class of finite-perimeter sets and hence up to a Lebesgue-negligible set. The local regularity of u can be described in terms of the distance of any two of its level sets. This is the main idea in [20] which can be refined to obtain the Hölder regularity of solutions of (14). As we argued in Section 3.1, outside the jump discontinuities of f (modulo an $\mathcal{H}^{N-1}$-null set), any two level sets at different heights cannot touch and hence the function u is continuous there. To be able to assert a Hölder type regularity property for u one needs to prove a local estimate of the distance of the boundaries of two level sets. This can be done here under the assumption of local Hölder regularity for f [21].

Theorem 3. *Let $N \leq 7$ and let u be a solution of (23). Assume that f is in $C^{0,\beta}$ locally in some open set $A \subseteq \Omega$, for some $\beta \in [0,1]$. Then u is also $C^{0,\beta}$ locally in A.*

The Lipschitz case corresponds to $\beta = 1$.

One can also state a global regularity result for solutions of the Neumann problem when $\Omega \subset \mathbb{R}^N$ is a convex domain. Let $f : \overline{\Omega} \to \mathbb{R}$ be a uniformly continuous function, with modulus of continuity $\omega_f : [0, +\infty) \to [0, +\infty)$, that is $|f(x) - f(y)| \leq \omega_f(|x - y|)$ for all $x, y \in \Omega$. We consider the solution u of (23) with homogeneous Neumann boundary condition, that is, such that (22) for any compact set $K \subset \overline{\Omega}$ and any $v \in BV(\Omega)$ such that $v = u$ out of K. This solution is unique, as can be shown adapting the proof of [19, Cor. C.2.] (see also [11] for the required adaptations to deal with the boundary condition), which deals with the case $\Omega = \mathbb{R}^N$.

Then, the following result holds true [21]:

Theorem 4. *Assume $N \leq 7$. Then, the function u is uniformly continuous in Ω, with modulus $\omega_u \leq \omega_f$.*

Again, is quite likely here that the assumption $N \leq 7$ is not necessary for this result.

4 Some explicit solutions

Recall that a convex body in $\mathbb{R}^N$ is a compact convex subset of $\mathbb{R}^N$. We say that a convex body is non-trivial if it has nonempty interior.

We want to exhibit the explicit solution of (13) when $f = \chi_C$ and C is a non-trivial convex body in $\mathbb{R}^N$. This will show that the preservation of a jump discontinuity depends on the curvature of ∂C at the given point, the size of the jump and the regularization parameter λ.

Let $u_{\lambda,C}$ be the unique solution of the problem:

$$\min_{u \in BV(\mathbb{R}^N)} \int_{\mathbb{R}^N} |Du| + \frac{1}{2\lambda} \int_{\mathbb{R}^N} (u - \chi_C)^2 \, dx \,. \tag{24}$$

The following result was proved in [7].

Proposition 4.1. *We have that $0 \leq u_{\lambda,C} \leq 1$, $u_{\lambda,C} = 0$ in $\mathbb{R}^N \setminus C$ and $u_{\lambda,C}$ is concave in $\{u_{\lambda,C} > 0\}$.*

The proof of $0 \leq u_{\lambda,C} \leq 1$ follows from a weak version of the maximum principle [7]. Thanks to the convexity of C, by comparison with the characteristic function of hyperplanes one can show that $u_{\lambda,C} = 0$ out of C [7]. To prove that $u_{\lambda,C}$ is concave in $\{u_{\lambda,C} > 0\}$ one considers first the case where C is of class $C^{1,1}$ and $\lambda > 0$ is small enough. Then one proves that $u_{\lambda,C}$ is concave by approximating $u_{\lambda,C}$ by the solution u_ϵ of

$$\begin{aligned} u - \lambda \mathrm{div} \left(\frac{\nabla u}{\sqrt{\epsilon^2 + |\nabla u|^2}} \right) &\qquad \text{in } C \\ \frac{\nabla u}{\sqrt{\epsilon^2 + |\nabla u|^2}} \cdot \nu^C = 0 &\qquad \text{in } \partial C, \end{aligned} \tag{25}$$

as $\epsilon \to 0+$, using Korevaar's concavity Theorem [48]. Then one considers the case where C is of class $C^{1,1}$ and we take any $\lambda > 0$. In this case, the concavity of $u_{\lambda,C}$ in $\{u_{\lambda,C} > 0\}$ is derived after proving Theorems 5 and 6 below. The final step proceeds by approximating a general convex body C by convex bodies of class $C^{1,1}$ [5].

Moreover, since $u_{\lambda,C} = 0$ out of C, the upper level set $\{u_{\lambda,C} > s\} \subseteq C$ for any $s \in (0,1]$. Then, as in Proposition 3.1, one can prove that for any $s \in (0,1]$ the level set $\{u_{\lambda,C} > s\}$ is a solution of

$$(P)_\mu \qquad \min_{E \subseteq C} P(E) - \mu|E|. \tag{26}$$

for the value of $\mu = \lambda^{-1}(1-s)$. When taking $\lambda \in (0,+\infty)$ and $s \in (0,1]$ we are able to cover the whole range of $\mu \in [0,\infty)$ [7]. By Lemma 3.2 we know that if $\mu < \mu'$ and $C_\mu, C_{\mu'}$ are minimizers of $(P)_\mu$, $(P)_{\mu'}$, respectively, then $C_\mu \subseteq C_{\mu'}$. This implies that the solution of $(P)_\mu$ is unique for any value $\mu \in (0,\infty)$ up to a countable exceptional set. Thus the sets C_μ can be identified with level sets of $u_{\lambda,C}$ for some $\lambda > 0$ and, therefore, we obtain its uniqueness from the concavity of $u_{\lambda,C}$. One can prove [7, 18, 5]:

Theorem 5. *There is a value $\mu^* > 0$ such that*

$$\begin{cases} \text{if } \mu < \mu^*, \ C_\mu = \emptyset, \\ \text{if } \mu > \mu^*, \ C_\mu \ \text{ is unique (and convex),} \\ \text{if } \mu = \mu^*, \ \ \text{there are two solutions } \emptyset \text{ and } C_{\mu^*}, \end{cases}$$

where C_{μ^*} is the unique Cheeger set of C. Moreover for any $\lambda < \|\chi_C\|_*$ we have $\mu^* := \frac{1-\|u_{\lambda,C}\|_\infty}{\lambda}$ and $C_\mu := \{u_{\lambda,C} > 1 - \mu\lambda\}$ for any $\mu > \mu^*$, where

$$\|\chi_C\|_* := \max\left\{ \int_{\mathbb{R}^N} u\,\chi_C\,dx : \ u \in BV(\mathbb{R}^N), \ \int_{\mathbb{R}^N} |Du| \le 1 \right\}.$$

The set C_{μ^*} coincides with the level set $\{u_{\lambda,C} = \|u_{\lambda,C}\|_\infty\}$ and is of class $C^{1,1}$.

We call a Cheeger set in a nonempty open bounded subset Ω of $\mathbb{R}^N$ any set $G \subseteq \Omega$ which minimizes

$$\mathcal{C}_\Omega \ := \ \min_{F \subseteq \Omega} \frac{P(F)}{|F|}. \tag{27}$$

The Theorem contains the assertion that there is a unique Cheeger set in any nonempty convex body of $\mathbb{R}^N$ and $\mu^* = \mathcal{C}_\Omega$. This result was proved in [18] for uniformly convex bodies of class C^2, and in [5] in the general case. Notice that the solution of (24) gives a practical algorithm to compute the Cheeger set of C.

Theorem 6. *Let C be a non-trivial convex body in $\mathbb{R}^N$. Let*

$$H_C(x) := \begin{cases} -\inf\{\mu : x \in C_\mu\} & \text{if} \quad x \in C \\ 0 & \text{if} \quad x \in \mathbb{R}^N \setminus C. \end{cases}$$

Then $u_{\lambda,C}(x) := (1 + \lambda H_C(x))^+ \chi_C$.

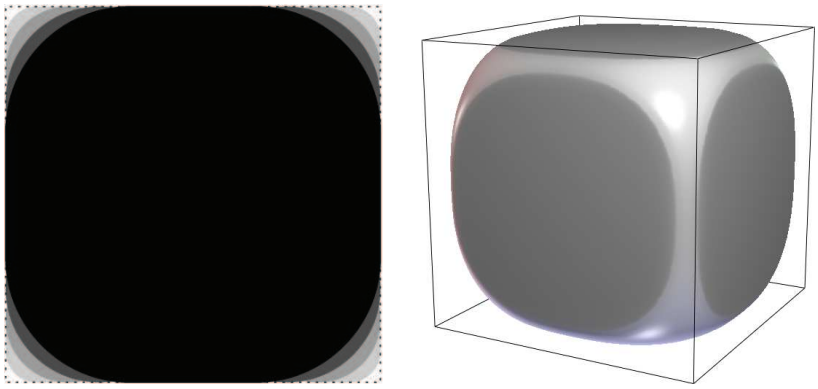

Figure 1: Left: The denoising of a square. Right: The Cheeger set of a cube.

If $N = 2$ and $\mu > \mu^*$, the set C_μ coincides with the union of all balls of radius $1/\mu$ contained in C [6]. Thus its boundary outside ∂C is made by arcs of circle which are tangent to ∂C. In particular, if C is a square, then the Cheeger set corresponds to the arcs of circle with radius $R > 0$ such that $\frac{P(C_{\mu^*})}{|C_{\mu^*}|} = \frac{1}{R}$. We can see that the corners of C are rounded and the discontinuity disappears as soon as $\lambda > 0$ (see the left part of Figure 1). This is a general fact at points of ∂C where its mean curvature is infinite.

Remark 4.2. By adapting the proof of Proposition 4 in [7] one can prove the following result. If Ω is a bounded subset of $\mathbb{R}^N$ with Lipschitz continuous boundary, and $u \in BV(\Omega) \cap L^2(\Omega)$ is the solution of the variational problem

$$\min_{u \in BV(\Omega) \cap L^2(\Omega)} \left\{ \int_\Omega |Du| + \frac{1}{2\lambda} \int_\Omega (u-1)^2 \, dx + \int_{\partial\Omega} |u| \, d\mathcal{H}^{N-1} \right\}, \tag{28}$$

then $0 \leq u \leq 1$ and for any $s \in (0, 1]$ the upper level set $\{u \geq s\}$ is a solution of

$$\min_{F \subseteq \Omega} P(F) - \lambda^{-1}(1-s)|F|. \tag{29}$$

If $\lambda > 0$ is big enough, indeed greater than $1/\|\chi_\Omega\|_*$, then the level set $\{u = \|u\|_\infty\}$ is the maximal Cheeger set of Ω. In particular, the maximal Cheeger set can be computed by solving (28), and for that we can use the algorithm in [25] described in Section 5.2. In the right side of Figure 1 we display the Cheeger set of a cube.

Other explicit solutions corresponding to the union of convex sets can be found in [14, 2]. In particular, Allard [2] describes the solution corresponding to the union of two discs in the plane and also the case of two squares with parallel sides touching by a vertex. Some explicit solutions for functions whose level sets are a finite number of convex sets in $\mathbb{R}^2$ can be found in [15].

5 Numerical algorithms: iterative methods

5.1 Notation

Let us fix our main notations. We denote by X the Euclidean space $\mathbb{R}^{N\times N}$. The Euclidean scalar product and the norm in X will be denoted by $\langle\cdot,\cdot\rangle_X$ and $\|\cdot\|_X$, respectively. Then the image $u \in X$ is the vector $u = (u_{i,j})_{i,j=1}^N$, and the vector field ξ is the map $\xi : \{1,\dots,N\}\times\{1,\dots,N\} \to \mathbb{R}^2$. To define the discrete total variation, we define a discrete gradient operator. If $u \in X$, the discrete gradient is a vector in $Y = X \times X$ given by

$$\nabla u := (\nabla_x u, \nabla_y u),$$

where

$$(\nabla_x u)_{i,j} = \begin{cases} u_{i+1,j} - u_{i,j} & \text{if} \quad i < N \\ 0 & \text{if} \quad i = N, \end{cases} \tag{30}$$

$$(\nabla_y u)_{i,j} = \begin{cases} u_{i,j+1} - u_{i,j} & \text{if} \quad j < N \\ 0 & \text{if} \quad j = N \end{cases} \tag{31}$$

for $i, j = 1,\dots,N$. Notice that the gradient is discretized using forward differences and $\nabla^{+,+}u$ could be a more explicit notation. For simplicity we have preferred to use ∇u. Other choices of the gradient are possible, this one will be convenient for the developments below.

The Euclidean scalar product in Y is defined in the standard way by

$$\langle \xi, \tilde{\xi}\rangle_Y = \sum_{1\le i,j\le N} (\xi^1_{i,j}\tilde{\xi}^1_{i,j} + \xi^2_{i,j}\tilde{\xi}^2_{i,j})$$

for every $\xi = (\xi^1, \xi^2)$, $\tilde{\xi} = (\tilde{\xi}^1, \tilde{\xi}^2) \in Y$. The norm of $\xi = (\xi^1, \xi^2) \in Y$ is, as usual, $\|\xi\|_Y = \langle \xi, \xi\rangle_Y^{1/2}$. We denote the euclidean norm of a vector $v \in \mathbb{R}^2$ by $|v|$. Then the discrete total variation is

$$J_d(u) = \|\nabla u\|_Y = \sum_{1\le i,j\le N} |(\nabla u)_{i,j}|. \tag{32}$$

We have

$$J_d(u) = \sup_{\xi\in Y,\, |\xi_{i,j}|\le 1\, \forall (i,j)} \langle \xi, \nabla u\rangle_Y. \tag{33}$$

By analogy with the continuous setting, we introduce a discrete divergence div as the dual operator of ∇, i.e., for every $\xi \in Y$ and $u \in X$ we have

$$\langle -\operatorname{div}\xi, u\rangle_X = \langle \xi, \nabla u\rangle_Y.$$

One can easily check that div is given by

$$\begin{aligned} (\operatorname{div}\xi)_{i,j} \quad = \quad & \begin{cases} \xi^1_{i,j} - \xi^1_{i-1,j} & \text{if} \quad 1 < i < N \\ \xi^1_{i,j} & \text{if} \quad i = 1 \\ -\xi^1_{i-1,j} & \text{if} \quad i = N \end{cases} \\ + \quad & \begin{cases} \xi^2_{i,j} - \xi^2_{i,j-1} & \text{if} \quad 1 < j < N \\ \xi^2_{i,j} & \text{if} \quad j = 1 \\ -\xi^2_{i,j-1} & \text{if} \quad j = N \end{cases} \end{aligned} \tag{34}$$

for every $\xi = (\xi^1, \xi^2) \in Y$.

We have

$$J_d(u) := \max_{\xi \in \mathcal{V}} \langle u, \operatorname{div} \xi \rangle, \tag{35}$$

where

$$\mathcal{V} = \{\xi \in Y : |\xi_{i,j}|^2 - 1 \leq 0, \ \forall\, i,j \in \{1,\dots,N\}\}$$

5.2 Chambolle's algorithm

Let us describe the dual formulation for solving the problem:

$$\min_{u \in X} \quad J_d(u) + \frac{1}{2\lambda}\|u - f\|_X^2 \tag{36}$$

where $f \in X$. Using (35) we have

$$\begin{aligned} \min_{u \in X} J_d(u) + \frac{1}{2\lambda}\|u - f\|_X^2 &= \min_{u \in X} \max_{\xi \in \mathcal{V}} \langle u, \operatorname{div} \xi \rangle + \frac{1}{2\lambda}\|u - f\|_X^2 \\ &= \max_{\xi \in \mathcal{V}} \min_{u \in X} \langle u, \operatorname{div} \xi \rangle + \frac{1}{2\lambda}\|u - f\|_X^2. \end{aligned}$$

Solving explicitly the minimization in u, we have $u = f - \lambda \operatorname{div} \xi$. Then

$$\begin{aligned} \max_{\xi \in \mathcal{V}} \min_{u \in X} \langle u, \operatorname{div} \xi \rangle + \frac{1}{2\lambda}\|u - f\|_X^2 &= \max_{\xi \in \mathcal{V}} \langle f, \operatorname{div} \xi \rangle - \frac{\lambda}{2}\|\operatorname{div} \xi\|_X^2 \\ &= -\frac{\lambda}{2} \min_{\xi \in \mathcal{V}} \left(\left\| \operatorname{div} \xi - \frac{f}{\lambda} \right\|_X^2 - \left\| \frac{f}{\lambda} \right\|_X^2 \right). \end{aligned}$$

Thus if ξ^* is the solution of

$$\min_{\xi \in \mathcal{V}} \left\| \operatorname{div} \xi - \frac{f}{\lambda} \right\|_X^2. \tag{37}$$

then $u = f - \lambda \operatorname{div} \xi^*$ is the solution of (36).

Notice that $\operatorname{div} \xi^*$ is the projection of $\frac{f}{\lambda}$ onto the convex set

$$K_d := \{\operatorname{div} \xi : |\xi_{i,j}| \leq 1, \ \forall\, i,j \in \{1,\dots,N\}\}.$$

As in [25], the Karush-Kuhn-Tucker Theorem yields the existence of Lagrange multipliers $\alpha_{i,j} \geq 0$ for the constraints $\xi \in \mathcal{V}$, such that we have for each $(i,j) \in \{1,\dots,N\}^2$

$$\nabla[\operatorname{div} \xi - \lambda^{-1} f]_{i,j} - \alpha^*_{i,j} \xi_{i,j} = 0, \tag{38}$$

with either $\alpha^*_{i,j} > 0$ and $|\xi_{i,j}| = 1$, or $\alpha^*_{i,j} = 0$ and $|\xi_{i,j}| \leq 1$. In the later case, we have $\nabla[\operatorname{div} \xi - \lambda^{-1} f]_{i,j} = 0$. In any case, we have

$$\alpha^*_{i,j} = |\nabla[\operatorname{div} \xi - \lambda^{-1} f]_{i,j}|. \tag{39}$$

Let $\nu > 0$, $\xi^0 = 0$, $p \geq 0$. We solve (38) using the following gradient descent (or fixed point) algorithm

$$\xi^{p+1}_{i,j} = \xi^p_{i,j} + \nu \nabla[\operatorname{div} \xi^p - \lambda^{-1} f]_{i,j} - \nu |\nabla[\operatorname{div} \xi^p - \lambda^{-1} f]_{i,j}| \xi^{p+1}_{i,j}, \tag{40}$$

Figure 2: Denoising results obtained with Chambolle's algorithm. a) Top left: the original image. b) Top right: the image with a Gaussian noise of standard deviation $\sigma = 10$. c) Bottom left: the result obtained with $\lambda = 5$. d) Bottom right: the result obtained with $\lambda = 10$.

hence

$$\xi_{i,j}^{p+1} = \frac{\xi_{i,j}^{p} + \nu \nabla[\operatorname{div} \xi^{p} - \lambda^{-1} f]_{i,j}}{1 + \nu |\nabla[\operatorname{div} \xi^{p} - \lambda^{-1} f]_{i,j}|}. \tag{41}$$

Observe that $|\xi_{i,j}^{p}| \leq 1$ for all $i, j \in \{1, \ldots, N\}$ and every $p \geq 0$.

Theorem 7. *In the discrete framework, assuming that $\nu < \frac{1}{8}$, then $\operatorname{div} \xi^{p}$ converges to the projection of $\frac{f}{\lambda}$ onto the convex set K_d. If $\operatorname{div} \xi^{*}$ is that projection, then $u = f - \lambda \operatorname{div} \xi^{*}$ is the solution of (36).*

In Figure 2 we display some results obtained using Chambolle's algorithm with different set of parameters, namely $\lambda = 5, 10$.

Today, the algorithms of Nesterov [51] or Beck and Teboulle [13] provide more efficient way to solve this dual problem.

5.3 Primal-dual approaches

The primal gradient descent formulation is based on the solution of (36). The dual gradient descent algorithm corresponds to (41). The primal-dual formulation is based on the formulation

$$\min_{u\in X}\max_{\xi\in\mathcal{V}} G(u,\xi) := \langle u, \operatorname{div}\xi\rangle + \frac{1}{2\lambda}\|u-f\|_X^2$$

and performs a gradient descent in u and gradient ascent in ξ.

Given the intermediate solution (u^k,ξ^k) at iteration step k we update the dual variable by solving

$$\max_{\xi\in\mathcal{V}} G(u^k,\xi). \tag{42}$$

Since the gradient ascent direction is $\nabla_\xi G(u^k,\xi) = -\nabla u^k$, we update ξ as

$$\xi^{k+1} = P_{\mathcal{V}}(\xi^k - \frac{\tau_k}{\lambda}\nabla u^k), \tag{43}$$

where τ_k denotes the dual stepsize and $P_{\mathcal{V}}$ denotes the projection onto the convex set $\mathcal{V}$. The projection $P_{\mathcal{V}}$ can be computed as in (41) or simply as

$$(P_{\mathcal{V}}\xi)_{i,j} = \frac{\xi_{i,j}}{\max(|\xi_{i,j}|,1)}.$$

Now we update the primal variable u by a gradient descent step of

$$\min_{u\in X} G(u,\xi^{k+1}). \tag{44}$$

The gradient ascent direction is $\nabla_u G(u,\xi^{k+1})$ and the update is

$$u^{k+1} = u^k - \theta_k\left(\lambda\operatorname{div}\xi^{k+1} + u^k - f\right), \tag{45}$$

where θ_k denotes the primal stepsize.

The primal-dual scheme was introduced in [60] where the authors observed its excellent performance although, as they point out, there is no global convergence proof. The convergence is empirically observed for a variety of suitable stepsize pairs (τ,θ) and is given in terms of the product $\tau\theta$. For instance, convergence is reported for increasing values θ_k and $\tau_k\theta_k \le 0.5$, see [60].

The primal gradient descent and the dual projected gradient descent method are special cases of the above algorithm. Indeed if one solves the problem (42) exactly (taking $\tau_k = \infty$ in (43)) the resulting algorithm is

$$u^{k+1} = u^k - \theta_k\left(-\lambda\operatorname{div}\frac{\nabla u^k}{|\nabla u^k|} + u^k - f\right), \tag{46}$$

with the implicit convention that we may take any element in the unit ball of $\mathbb{R}^2$ when $\nabla u^k = 0$.

If we solve (44) exactly and still apply gradient ascent to (42), the resulting algorithm is

$$\xi^{k+1} = P_{\mathcal{V}}\left(\xi^k + \tau_k\nabla(\operatorname{div}\xi^k - \frac{f}{\lambda})\right), \tag{47}$$

which essentially corresponds to (41).

The primal-dual approach can be extended to the total variation deblurring problem

$$\min_{u\in X} \quad J_d(u) + \frac{1}{2\lambda}\|Bu - f\|_X^2 \tag{48}$$

where $f \in X$ and B is a matrix representing the discretization of the blurring operator H.

The primal-dual scheme is based on the formulation

$$\min_{u\in X}\max_{\xi\in\mathcal{V}} \quad \langle u, \operatorname{div}\xi\rangle + \frac{1}{2\lambda}\|Bu - f\|_X^2, \tag{49}$$

and the numerical scheme can be written as

$$\begin{aligned} \xi^{k+1} &= P_{\mathcal{V}}\left(\xi^k - \tau_k \nabla u^k\right) \\ u^{k+1} &= u^k - \theta^k\left(-\operatorname{div}\xi^{k+1} + \lambda B^t(Bu^{k+1} - f)\right). \end{aligned} \tag{50}$$

Since B is the matrix of a convolution operator, the second equation can be solved explicitly using the FFT. Again, convergence is empirically observed for a variety of suitable stepsize pairs (τ, θ) and is given in terms of the product $\tau\theta$, see [60].

For a detailed study of different primal-dual methods we refer to [39].

6 Numerical algorithms: maximum flow methods

It has been noticed probably first in [53] that maximal flow/minimum cut techniques could be used to solve discrete problems of the form (14), that is, to compute finite sets minimizing a discrete variant of the perimeter and an additional external field term. Combined with (a discrete equivalent of) Proposition 3.1, this leads to efficient techniques for solving (only) the denoising problem (8), including a method, due to D. Hochbaum, to compute an exact solution in polynomial time (up to machine precision). A slightly more general problem is considered in [28], where the authors describe in detail algorithms which solve the problem with an arbitrary precision.

6.1 Discrete perimeters and discrete total variation

We will call a discrete total variation any convex, nonnegative function $J : \mathbb{R}^M \to [0, +\infty]$ satisfying a discrete *co-area* formula:

$$J(u) \;=\; \int_{-\infty}^{+\infty} J(\chi^{\{u\geq s\}})\, ds \tag{51}$$

where $\chi^{\{u\geq s\}} \in \{0,1\}^M$ denotes the vector such that $\chi_i^{\{u\geq s\}} = 0$ if $u_i \leq s$ and $\chi_i^{\{u\geq s\}} = 1$ if $u_i \geq s$.

As an example we can consider the (anisotropic) discrete total variation

$$J(u) \;=\; \sum_{\substack{1\leq i<N\\ 1\leq j\leq N}} |u_{i+1,j} - u_{i,j}| + \sum_{\substack{1\leq i\leq N\\ 1\leq j<N}} |u_{i,j+1} - u_{i,j}| \tag{52}$$

In this case $u = (u_{i,j})_{i,j=1}^N$ can be written as a vector in $\mathbb{R}^M$ with $M = N^2$. Then, (51) obviously holds since for any $a, b \in \mathbb{R}$, we have $|a - b| = \int_{-\infty}^{+\infty} |\chi_{\{a>s\}} - \chi_{\{b>s\}}| \, ds$.

Observe, on the other hand, that the discretization (36) does not enter this category (unfortunately). In fact, a discrete total variation will be always very anysotropic (or "crystalline").

We assume that J is not identically $+\infty$. Then, we can derive from (51) the following properties [28]:

Proposition 6.1. *Let J be a discrete total variation. Then:*

1. *J is positively homogeneous: $J(\lambda u) = \lambda J(u)$ for any $u \in \mathbb{R}^M$ and $\lambda \geq 0$.*
2. *J is invariant by addition of a constant: $J(c\mathbf{1} + u) = J(u)$ for any $u \in \mathbb{R}^M$ and $c \in \mathbb{R}$, where $\mathbf{1} = (1, \ldots, 1) \in \mathbb{R}^M$ is a constant vector. In particular, $J(\mathbf{1}) = 0$.*
3. *J is lower-semicontinuous.*
4. *$p \in \partial J(u) \Leftrightarrow (\forall z \in \mathbb{R}, p \in \partial J(\chi^{\{u \geq z\}})$.*
5. *J is* submodular*: for any $u, u' \in \{0,1\}^M$,*

$$J(u \vee u') + J(u \wedge u') \leq J(u) + J(u'). \tag{53}$$

More generally, this will hold for any $u, u' \in \mathbb{R}^M$.

Conversely, if $J : \{0,1\}^M \to [0, +\infty]$ is a submodular function with $J(0) = J(\mathbf{1}) = 0$, then the co-area formula (51) extends it to $\mathbb{R}^M$ into a convex function, hence a discrete total variation.

If J is a discrete total variation, then the discrete counterpart of Proposition 3.1 holds:

Proposition 6.2. *Let J be a discrete total variation. Let $f \in \mathbb{R}^M$ and let $u \in \mathbb{R}^M$ be the (unique) solution of*

$$\min_{u \in \mathbb{R}^M} \lambda J(u) + \frac{1}{2}\|u - f\|^2 \tag{54}$$

Then, for all $s > 0$, the characteristic functions of the super-level sets $E_s = \{u \geq s\}$ and $E'_s = \{u > s\}$ (which are different only if $s \in \{u_i, i = 1, \ldots, M\}$) are respectively the largest and smallest minimizer of

$$\min_{\theta \in \{0,1\}^M} \lambda J(\theta) + \sum_{i=1}^M \theta_i (s - f_i) \, . \tag{55}$$

The proof is quite clear, since the only properties which were used for showing Proposition 3.1 where (a) the co-area formula of Theorem 1; (b) the submodularity of the perimeters (10).

As a consequence, Problem (54) can be solved by successive minimizations of (55), which in turn can be done by computing a maximal flow through a graph, as will be explained in the next section. It seems that efficiently solving the successive minimizations has been first

proposed in the seminal work of Eisner and Severance [38] in the context of augmenting-path maximum-flow algorithms. It was then developed, analyzed and improved by Gallo, Grigoriadis and Tarjan [40] for preflow-based algorithms. Successive improvements were also proposed by Hochbaum [44], specifically for the minimization of (54). We also refer to [27, 33] for variants, and to [46] for detailed discussions about this approach.

6.2 Graph representation of energies for binary MRF

It was first observed by Picard and Ratliff [53] that binary Ising-like energies, that is, of the form

$$\sum_{i,j} \alpha_{i,j} |\theta_i - \theta_j| \, - \, \sum_i \beta_i \theta_i \, , \tag{56}$$

$\alpha_{i,j} \geq 0$, $\beta_i \in \mathbb{R}$, $\theta_i \in \{0,1\}$, could be represented on a graph and minimized by standard optimization techniques, and more precisely using maximum flow algorithms. Kolmogorov and Zabih [47] showed that the submodularity of the energy is a necessary condition, while, up to sums of ternary submodular interactions, it is also a sufficient condition in order to be representable on a graph. (But other energies are representable, and it does not seem to be known whether any submodular J can be represented on a graph, see [28, Appendix B] and the references therein.)

In case $J(u)$ has only pairwise interactions, as in (52), then Problem (55) has exactly the form (56), with $\alpha_{i,j} = \lambda$ if nodes i and j correspond to neighboring pixels, 0 else, and β_i is $s - f_i$.

Let us build a graph as follows: we consider $\mathcal{V} = \{1, \ldots, M\} \cup \{S\} \cup \{T\}$ where the two special nodes S and T are respectively called the "source" and the "sink". We consider then oriented edges (S,i) and (i,T), $i = 1, \ldots, M$, and (i,j), $1 \leq i,j \leq M$, and to each edge we associate a capacity defined as follows:

$$\begin{cases} c(S,i) \;=\; \beta_i^- & i = 1, \ldots, M \, , \\ c(i,T) \;=\; \beta_i^+ & i = 1, \ldots, M \, , \\ c(i,j) \;=\; \alpha_{i,j} & 1 \leq i,j \leq M \, . \end{cases} \tag{57}$$

Here $\beta_i^+ = \max\{0, \beta_i\}$ and $\beta_i^- = \max\{0, -\beta_i\}$, so that $\beta_i = \beta_i^+ - \beta_i^-$. By convention, we consider there is no edge between two nodes if the capacity is zero. Let us denote by $\mathcal{E}$ the set of edges with nonzero capacity and by $\mathcal{G} = (\mathcal{V}, \mathcal{E})$ the resulting oriented graph.

We then define a "cut" in the graph as a partition of $\mathcal{E}$ into two sets $\mathcal{S}$ and $\mathcal{T}$, with $S \in \mathcal{S}$ and $T \in \mathcal{T}$. The cost of a cut is then defined as the total sum of the capacities of the edges that start on the source-side of the cut and land on the sink-side:

$$C(\mathcal{S}, \mathcal{T}) \;=\; \sum_{\substack{(\mu,\nu) \in \mathcal{E} \\ \mu \in \mathcal{S}, \nu \in \mathcal{T}}} c(\mu, \nu) \, .$$

Then, if we let $\theta \in \{0,1\}^M$ be the characteristic function of $\mathcal{S} \cap \{1,\dots,M\}$, we have

$$\begin{aligned} C(\mathcal{S},\mathcal{T}) &= \sum_{i=1}^{M}(1-\theta_i)\beta_i^- + \theta_i\beta_i^+ + \sum_{i,j=1}^{M}\alpha_{i,j}(\theta_i-\theta_j)^+ \\ &= \sum_{i,j=1}^{M}\alpha_{i,j}(\theta_i-\theta_j)^+ + \sum_{i=1}^{M}\theta_i\beta_i + \sum_{i=1}^{M}\beta_i^- \end{aligned}$$

If $\alpha_{i,j} = \alpha_{j,i}$ (but other situations are also interesting), this is nothing else than energy (56), up to a constant.

Thus, the problem of finding a minimum of (56) (or (55)) can be reformulated as the problem of finding a minimal cut in the graph. Very efficient algorithms are available, based on a duality result of Ford and Fulkerson [1]. It states that the maximum flow on the graph constrained by the capacities of the edges is equal to the minimal cost of a cut. The problem reduces then to find the maximum flow in the graph. This is precisely defined as follows: starting from S, we "push" a quantity $(x_{\mu,\nu})$ along the oriented edges $(\mu,\nu) \in \mathcal{E}$ of the graph, with the constraint that along each edge,

$$0 \;\leq\; x_{\mu,\nu} \;\leq\; c(\mu,\nu)$$

and that each "interior" node i must satisfy the flow conservation constraint

$$\sum_{\mu} x_{\mu,i} \;=\; \sum_{\mu} x_{i,\mu}$$

(while the source S only sends flow to the network, and the sink T only receives).

It is clear that the total flow $f(x) = \sum_i x_{S,i} = \sum_i x_{i,T}$ which can be sent is bounded from above, and not hard to show that a bound is given by a minimal-cost cut $(\mathcal{S},\mathcal{T})$. The duality theorem of Ford and Fulkerson expresses the fact that this bound is actually reached by the maximal flow $(x_{\mu,\nu})_{(\mu,\nu)\in\mathcal{E}}$ (which maximizes $f(x)$), and the partition $(\mathcal{S},\mathcal{T})$ is obtained by cutting along the saturated edges (μ,ν), where $x_{\mu,\nu} = c_{\mu,\nu}$ while $x_{\nu,\mu} = 0$.

We can find starting from S the first saturated edge along the graph, and cut there, or do the same starting from T and scanning the reverse graph: for $\beta_i = s - f_i$, this will usually give the same solution except for a finite number of levels s, which correspond exactly to the levels $\{u_i \,:\, i = 1,\dots,M\}$ of the solution of (54) and are called the "breakpoints".

Several efficient algorithms are available to compute a maximum flow in polynomial time [1]. Although the time complexity of the algorithm in [16], of Boykov and Kolmogorov, is not polynomial, this algorithm seems to outperform others in terms in time computations, as it is particularly designed for the graphs with low connectivity which arise in image processing.

The idea of a "parametric maximum flow algorithm" [40] is to re-use the same graph (and the "residual graph" which remains after a run of a max-flow algorithm) to solve problems (55) for increasing values $s \in \{s_0, s_1, \dots, s_n\}$. This is easily shown to solve (54) up to an arbitrary precision (and in polynomial time, see [40]). It seems this idea was already present in a paper of Eisner and Severance [38].

However, it was shown in [44] by D. Hochbaum that in fact the *exact* solution to (54) can be computed, also in polynomial time. Let us now explain the basic idea of this approach, for details we refer to [28, 44].

Let $u = (u_i)_{i=1}^M$ be the (unique) solution of (54). Proposition 6.2 tells us that as s varies, problem (55) has the same solution $\chi^{\{u \geq s\}}$ as long as s does not cross any of the values $\{u_i : i = 1, \dots, M\}$, which are precisely the breakpoints.

Assume we have found, for two levels $s_1 < s_2$, solutions $\theta^1 \geq \theta^2$ of (55) and assume also that these solutions differ. It means that there is a breakpoint u_{i_0} in between: there is at least one location i_0 (and possibly other) with $s_1 \leq u_{i_0} \leq s_2$.

Suppose for a while that the value u_{i_0} were the *only* breakpoint between s_1 and s_2 (that is, at no other location i_1, we can have both $s_1 \leq u_{i_1} \leq s_2$ and $u_{i_0} \neq u_{i_1}$).

In this case, for $s \in [s_1, s_2]$, the optimal energy should be

$$\mathcal{F}(s) \;=\; \mathcal{F}_1(s) \;=\; \left(\lambda J(\theta^1) - \sum_{i=1}^M \theta_i^1 f_i\right) \;+\; s \sum_{i=1}^M \theta_i^1$$

if $s \leq u_{i_0}$, and

$$\mathcal{F}(s) \;=\; \mathcal{F}_2(s) \;=\; \left(\lambda J(\theta^2) - \sum_{i=1}^M \theta_i^2 f_i\right) \;+\; s \sum_{i=1}^M \theta_i^2$$

for $s \geq u_{i_0}$. And the value u_{i_0} is necessary the (only) solution of the equation $\mathcal{F}_1(u_{i_0}) = \mathcal{F}_2(u_{i_0})$.

Observe that in any case, as $\theta^1 \geq \theta^2$ and they are different, the slope of the affine function $\mathcal{F}_1(s)$ is strictly above the slope of the affine function $\mathcal{F}_2(s)$. Since also $\mathcal{F}_1(s_1) \leq \mathcal{F}_2(s_1)$ (as θ^1 is optimal for s_1) and $\mathcal{F}_2(s_2) \leq \mathcal{F}_1(s_2)$, there is always a (unique) value $s_3 \in [s_1, s_2]$ for which $\mathcal{F}_1(s_3) = \mathcal{F}_2(s_3)$.

The idea of the algorithm is now clear: we have to compute a new maximal flow (which, in fact, re-uses the residual flows from the computations of θ^1 and θ^2) to solve (55) for the level $s = s_3$. We find a solution θ^3, of energy

$$\mathcal{F}_3(s_3) \;=\; \left(\lambda J(\theta^3) - \sum_{i=1}^M \theta_i^3 f_i\right) \;+\; s_3 \sum_{i=1}^M \theta_i^3$$

Then, there are two cases:

- Either $\mathcal{F}_3(s_3) = \mathcal{F}_1(s_3) = \mathcal{F}_2(s_3)$: in this case we have found a breakpoint, and there is no other in the interval $[s_1, s_2]$. Hence, the level sets $\{u \geq s\}$ have been found for all values $s \in [s_1, s_2]$: $\chi^{\{u \geq s\}} = \theta^1$ for $s \in [s_1, s_3]$ and θ^2 for $s \in [s_3, s_2]$.

- Or $\mathcal{F}_3(s_3) < \mathcal{F}_1(s_3) = \mathcal{F}_2(s_3)$. Then, in particular, it must be that the solution θ^3 differs from both θ^1 and θ^2 (otherwise the energies would be the same). Hence we can start again to try solving the problem at the levels s_4 and s_5 which solve $\mathcal{F}_1(s_4) = \mathcal{F}_3(s_4)$ and $\mathcal{F}_3(s_5) = \mathcal{F}_2(s_5)$. Now, since there are only a finite number of possible sets θ solving (55) (bounded by M, as the solutions are nonincreasing with s), this situation can occur at most a finite number of time, bounded by M.

In practice, this can be done in a very efficient way, using "residual graphs" to start the new maximal flow algorithms, and to compute efficiently the new levels where to cut (there is no need, in fact, to compute the values $\lambda J(\theta) + \sum_i \theta_i f_i$ and $\sum_i \theta_i$ for this). See [44, 28] for details.

For experimental results in the case of total variation denoising we refer to [27, 28, 33, 41].

7 Other problems: Anisotropic total variation models

7.1 Global solutions of geometric problems

The theory of anisotropic perimeters developed in [8] permits to extend model (28) to general anisotropic perimeters, including as particular cases the geodesic active contour model with an inflating force [23, 45], and a model for edge linking [22]. This permits to find the global minima of geometric problems that appear in image processing [31, 22, 26, 28].

The anisotropic total variation and perimeter. Let us define the general notion of total variation with respect to an anisotropy. Following [8] we say that a function $\phi : \Omega \times \mathbb{R}^N \to [0, \infty)$ is a *metric integrand* if ϕ is a Borel function satisfying the conditions:

$$\text{for a.e. } x \in \Omega, \text{ the map } \xi \in \mathbb{R}^N \to \phi(x, \xi) \text{ is convex,} \tag{58}$$

$$\phi(x, t\xi) = |t|\phi(x, \xi) \qquad \forall x \in \Omega, \quad \forall \xi \in \mathbb{R}^N, \quad \forall t \in \mathbb{R}, \tag{59}$$

and there exists a constant $\Lambda > 0$ such that

$$0 \le \phi(x, \xi) \le \Lambda \|\xi\| \qquad \forall x \in \Omega, \quad \forall \xi \in \mathbb{R}^N. \tag{60}$$

We could be more precise and use the term symmetric metric integrand, but for simplicity we use the term metric integrand. Recall that the polar function $\phi^0 : \Omega \times \mathbb{R}^N \to \mathbb{R} \cup \{+\infty\}$ of ϕ is defined by

$$\phi^0(x, \xi^*) = \sup\{\langle \xi^*, \xi \rangle : \xi \in \mathbb{R}^N \, \phi(x, \xi) \le 1\}. \tag{61}$$

The function $\phi^0(x, \cdot)$ is convex and lower semicontinuous.

Let

$$\mathcal{K}_\phi(\Omega) := \{\sigma \in X_\infty(\Omega) : \phi^0(x, \sigma(x)) \le 1 \text{ for a.e. } x \in \Omega, \, [\sigma \cdot \nu^\Omega] = 0\}.$$

Definition 7.1. *Let $u \in L^1(\Omega)$. We define the ϕ-total variation of u in Ω as*

$$\int_\Omega |Du|_\phi := \sup\left\{ \int_\Omega u \, \operatorname{div} \sigma \, dx : \sigma \in \mathcal{K}_\phi^\infty(\Omega) \right\}, \tag{62}$$

We set $BV_\phi(\Omega) := \{u \in L^1(\Omega) : \int_\Omega |Du|_\phi < \infty\}$ which is a Banach space when endowed with the norm $|u|_{BV_\phi(\Omega)} := \int_\Omega |u| dx + \int_\Omega |Du|_\phi$.

We say that $E \subseteq \mathbb{R}^N$ has finite ϕ-perimeter in Ω if $\chi_E \in BV_\phi(\Omega)$. We set

$$P_\phi(E, \Omega) := \int_\Omega |D\chi_E|_\phi.$$

If $\Omega = \mathbb{R}^N$, we denote $P_\phi(E) := P_\phi(E, \mathbb{R}^N)$. By assumption (60), if $E \subseteq \mathbb{R}^N$ has finite perimeter in Ω it has also finite ϕ-perimeter in Ω.

A variational problem and its connection with geometric problems. Let $\phi : \Omega \times \mathbb{R}^N \to \mathbb{R}$ be a metric integrand in Ω and $h \in L^\infty(\Omega)$, $h(x) > 0$ a.e., with $\int_\Omega \frac{1}{h(x)}\, dx < \infty$. Let us consider the problem

$$\min_{u \in BV_\phi(\Omega)} \int_\Omega |Du|_\phi + \int_{\partial\Omega} \phi(x, \nu^\Omega)|u|\, d\mathcal{H}^{N-1} + \frac{\lambda}{2} \int_\Omega h\,(u-f)^2\, dx, \tag{63}$$

where ν^Ω denotes the outer unit normal to $\partial\Omega$. To shorten the expressions inside the integrals we shall write h, u instead of $h(x), u(x)$, with the only exception of $\phi(x, \nu^\Omega)$. The following result was proved in [22].

Theorem 8. *(i) Let $f \in L^2(\Omega, h dx)$, i.e., $\int_\Omega f(x)^2\, h(x)\, dx < \infty$. Then there is a unique solution of the problem (63).*

(ii) If $u \in BV_\phi(\Omega) \cap L^2(\Omega, h\, dx)$ be the solution of the variational problem (63) with $f = 1$. Then $0 \le u \le 1$ and the level sets $E_s := \{x \in \Omega : u(x) \ge s\}$, $s \in (0, 1]$, are solutions of

$$\min_{F \subseteq \Omega} P_\phi(F) - \mu |F|_h. \tag{64}$$

where $|F|_h = \int_F h(x)\, dx$. As in the euclidian case, the solution of (64) is unique for any $s \in (0, 1]$ up to a countable exceptional set.

(iii) When λ is big enough, the level set associated to the maximum of u, $\{u = \|u\|_\infty\}$, is the maximal (ϕ, h)-Cheeger set of Ω, i.e., is a minimizer of the problem

$$\inf \left\{ \frac{P_\phi(F)}{|F|_h} : F \subseteq \overline{\Omega} \text{ of finite perimeter}, |F|_h > 0 \right\}. \tag{65}$$

The computation of the maximal (ϕ, h)-Cheeger set (together with the solution of the family of problems (64)) can be computed by adapting Chambolle's algorithm [25] described in Section 5.2.

Examples. We illustrate this formalism with two examples: a) the geodesic active contour model; and b) a model for edge linking.

a) *The geodesic active contour model.* Let $I : \Omega \to \mathbb{R}^+$ be a given image in $L^\infty(\Omega)$, G be a Gaussian function, and

$$g(x) = \frac{1}{\sqrt{1 + |\nabla (G * I)|^2}}, \tag{66}$$

(where in $G * I$ we have extended I to $\mathbb{R}^N$ by taking the value 0 outside Ω). Observe that $g \in C(\overline{\Omega})$ and $\inf_{x \in \overline{\Omega}} g(x) > 0$. The geodesic active contour model [23, 45] with an inflating force corresponds to the case where $\phi(x, \xi) = g(x)|\xi|$ and $|Du|_\phi = g(x)|Du|$ and $h(x) = 1$, $x \in \Omega$. The purpose of this model is to locate the boundary of an object of the image at the points where the gradient is large. The presence of the inflating term helps to avoid minima collapsing into a point. The model was intially formulated [23, 45] in a level set framework

In this case we may write $P_g(F)$ instead of $P_\phi(F)$, and we have $P_g(F) := \int_{\partial^* F} g\, d\mathcal{H}^{N-1}$, where $\partial^* F$ is the reduced boundary of F [10].

In this case the Cheeger sets are a particular instance of geodesic active contour with an inflating force whose constant is $\mu = \mathcal{C}^{g,1}_\Omega$. An interesting feature of this formalism is that it permits to define local Cheeger sets as local (regional) maxima of the function u. They are Cheeger sets in a sub-domain of Ω. They can be identified with boundaries of the image and the above formalism permits to compute several active contours at the same time (the same holds true for the edge linking model).

b) *An edge linking model.* Another interesting application of the above formalism is to edge linking. Given a set $\Gamma \subseteq \Omega$ (which may be curves if $\Omega \subseteq \mathbb{R}^2$ or pieces of surface if $\Omega \subseteq \mathbb{R}^3$), we define $d_\Gamma(x) = \text{dist}(x, \Gamma)$ and the anisotropy $\phi(x, \xi) = d_\Gamma(x)|\xi|$. In that case, we experimentally see that the Cheeger set determined by this anisotropy links the set of curves (or surfaces) Γ. If Γ is a set of edges computed with an edge detector we obtain a set or curves ($N = 2$) or surfaces ($N = 3$) linking them.

Notice that, for a given choice of ϕ, we actually find many *local* ϕ-Cheeger sets, disjoint from the global minimum, that appear as local minima of the Cheeger ratio on the tree of connected components of upper level sets of u. The computation of those sets is partially justified by Proposition 6.11 in [22]. These are the sets which we show on the following experiments.

Let us mention the formulation of active contour models without edges proposed by Chan-Vese in [32] can also be related to the general formulation (64).

On Figure 3, we display some local ϕ-Cheeger sets of 2D images for the choices of metric ϕ corresponding to geodesic active contour models with an inflating force (the first three columns) and to edge linking problems (the last three columns). The first row displays the original images, the second row displays the metric $g = (\sqrt{1 + |\nabla(G * I)|^2})^{-1}$ or $g = d_S$. The last row displays the resulting segmentation or set of linked edges, respectively. Let us remark here a limitation of this approach, that can be observed in the last subfigure. Even if this linking is produced, the presence of a bottleneck (bottom right subfigure) makes the d_S-Cheeger set to be a set with large volume. This limitation can be circumvented by adding barriers in the domain Ω: we can enforce hard restrictions on the result by removing from the domain some points that we do not want to be enclosed by the output set of curves.

7.2 A convex formulation of continuous multi-label problems

Let us consider the variational problem

$$\min_{u \in BV(\Omega), 0 \leq u \leq M} \int_\Omega |Du| + \int_\Omega W(x, u(x))\, dx, \tag{67}$$

where $W : \Omega \times \mathbb{R} \to \mathbb{R}^+$ is a potential which is Borel measurable in x and continuous in u, but not necessarily convex. Thus the functional is nonlinear and non-convex. The functional can be relaxed to a convex one by considering the subgraph of u as an unknown.

Our purpose is to write the nonlinearities in (67) in a "convex way" by introducing a new auxiliary variable [54]. This will permit to use standard optimization algorithms. The

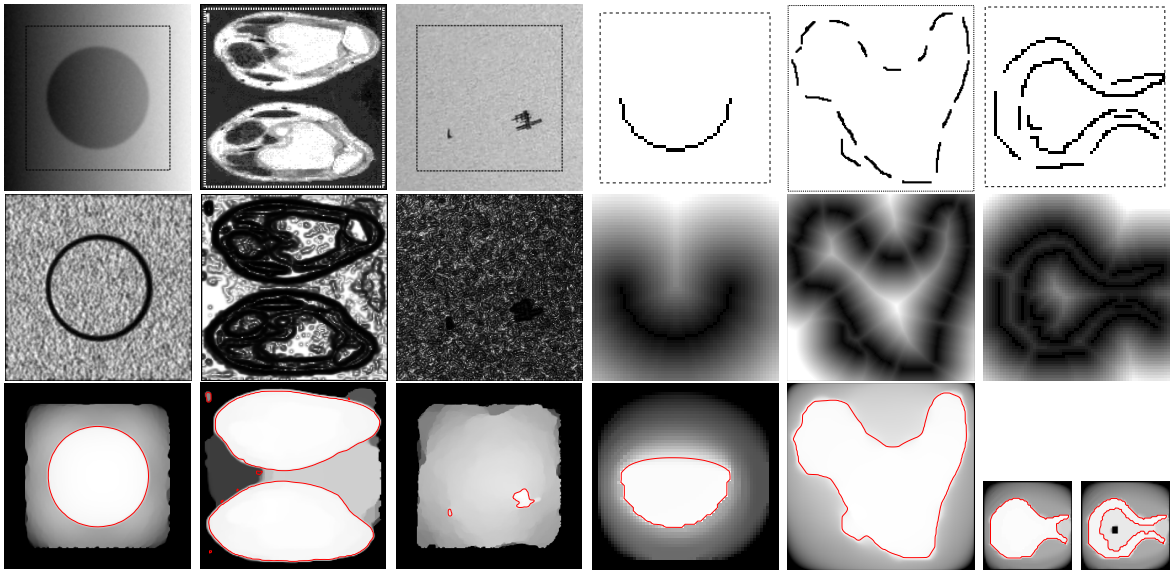

Figure 3: Geodesic active contours and edge linking experiments. The first row shows the images I to be processed. The first three columns correspond to segmentation experiments, the last three are edge linking experiments. The second row shows the weights g used for each experiment (white is 1, black is 0), in the first two cases $g = (\sqrt{1 + |\nabla(G * I)|^2})^{-1}$, for the third $g = 0.37(\sqrt{0.1 + |\nabla(G * I)|^2})^{-1}$ and for the linking experiments $g = d_S$, the scaled distance function to the given edges. The third row shows the disjoint minimum g-Cheeger sets extracted from u (shown in the background), there are 1,7,2,1,1 and 1 sets respectively. The last linking experiment illustrates the effect of introducing a barrier in the initial domain (black square).

treatment here will be heuristic.

Without loss of generality, let us assume that $M = 1$. Let $\phi(x, s) = H(u(x) - s)$, where $H = \chi_{[0,+\infty)}$ is the Heaviside function and $s \in \mathbb{R}$. Notice that the set of points where $u(x) > s$ (the subgraph of u) is identified as $\phi(x, s) = 1$. That is, $\phi(x, s)$ is an embedding function for the subgraphs of u. This permits to consider the problem as a binary set problem. The graphs of u is a 'cut' in ϕ.

Let

$$\mathcal{A} := \{\phi \in BV(\Omega \times [0, 1]) : \phi(x, s) \in \{0, 1\}, \forall (x, s) \in \Omega \times [0, 1]\}.$$

Using the definition of anisotropic total variation [8] we may write the energy in (67) in terms of ϕ as

$$\min_{\phi \in \mathcal{A}} \int_\Omega \int_0^1 \left(|D_x \phi| + W(x, s)|\partial_s \phi(x, s)|\right) \, dx \, dt + \int_\Omega (W(x, 0)|\phi(x, 0) - 1| + W(x, 1)|\phi(x, 1)|) \, dx, \tag{68}$$

where the boundary conditions $\phi(x, 0) = 1$, $\phi(x, 1) = 0$ are taken in a variational sense.

Although the energy (68) is convex in ϕ the problem is non-convex since the minimization is carried on $\mathcal{A}$ which is a non-convex set. The proposal in [54] is to relax the variational

problem by allowing ϕ to take values in $[0,1]$. This leads to the following class of admissible functionals

$$\widetilde{\mathcal{A}} := \{\phi \in BV(\Omega \times [0,1]) : \phi(x,s) \in [0,1],\ \forall (x,s) \in \Omega \times [0,1],\ \phi_s \leq 0\}. \tag{69}$$

The associated variational problem is written as

$$\min_{\phi \in \widetilde{\mathcal{A}}} \int_\Omega \int_0^1 \left(|D_x \phi| + W(x,s)|\partial_s \phi(x,s)|\right)\, dx\, dt + \int_\Omega (W(x,0)|\phi(x,0)-1| + W(x,1)|\phi(x,1)|)\, dx. \tag{70}$$

This problem is now convex and can be solved using the dual or primal-dual numerical schemes explained in Section 5.2 and 5.3. Formally, the level sets of a solution of (70) give solutions of (67). This can be proved using the developments in [8, 22].

In [29] the authors address the problem of convex formulation of multi-label problems with finitely many values including (67) and the case of non-convex neighborhood potentials like the Potts model or the truncated total variation. The general framework permits to consider the relaxation in $BV(\Omega)$ of functionals of the form

$$F(u) := \int_\Omega f(x, u(x), \nabla u(x))\, dx \tag{71}$$

where $u \in W^{1,1}(\Omega)$ and $f : \Omega \times \mathbb{R} \times \mathbb{R}^N \to [0, \infty[$ be a Borel function such that $f(x,z,\xi)$ is a convex function of ξ for any $(x,z) \in \Omega \times \mathbb{R}^N$ satisfying some coercivity assumption in ξ. Let f^* denote the Legendre-Fenchel conjugate of f with respect to ξ. If

$$K := \{\phi = (\phi^x, \phi^s) : \Omega \times \mathbb{R} \to \mathbb{R}^2 : \phi \text{ is smooth and } f^*(x,s,\phi^x(x,s)) \leq \phi^s(x,s)\}.$$

then the lower semicontinuous relaxation of F is

$$\mathcal{F}(u) = \sup_{\phi \in K} \int_\Omega \int_{\mathbb{R}} \phi \cdot D\chi_{\{(x,s):s<u(x)\}}.$$

Based on this formula one can use a dual or a primal-dual numerical scheme to minimize $\mathcal{F}(u)$ if one knows how to compute the projection onto the convex set K. We refer to [29] for details.

8 Other problems: Image restoration

To approach the problem of image restoration from a numerical point of view we shall assume that the image formation model incorporates the sampling process in a regular grid

$$f_{i,j} = (h * u)_{i.j} + n_{i,j}, \qquad (i,j) \in \{1, \ldots, N\}^2, \tag{72}$$

where $u : \mathbb{R}^2 \to \mathbb{R}$ denotes the ideal undistorted image, $h : \mathbb{R}^2 \to \mathbb{R}$ is a blurring kernel, f is the observed sampled image which is represented as a function $f : \{1, \ldots, N\}^2 \to \mathbb{R}$, and $n_{i,j}$ is, as usual, a white Gaussian noise with zero mean and standard deviation σ.

Let us denote by Ω_N the interval $[0, N[^2$. As we said in the introduction, in order to simplify this problem, we assume that h, u are functions defined in Ω_N and are periodic of

period N in each direction. To fix ideas, we assume that $h, u \in L^2(\Omega_N)$, so that $h * u$ is a continuous function in Ω_N and the samples $(h * u)_{i,j}$, $(i,j) \in \{1, \dots, N\}^2$, have sense.

Let us define the discrete functional

$$J_d^\beta(u) = \sum_{1 \le i,j \le N} \sqrt{\beta^2 + |(\nabla u)_{i,j}|^2}, \qquad \beta \ge 0.$$

For any function $w \in L^2(\Omega_N)$, its Fourier coefficients are

$$\hat{w}_{\frac{l}{N}, \frac{j}{N}} = \int_{\Omega_N} w(x,y) e^{-2\pi i \frac{(lx+jy)}{N}} \qquad \text{for } (l,j) \in \mathbb{Z}^2.$$

Our plan is to compute a band limited approximation to the solution of the restoration problem for (72). For that we define

$$\mathcal{B} := \{u \in L^2(\Omega_N) : \hat{u} \,\text{is supported in } \{-\tfrac{1}{2} + \tfrac{1}{N}, \dots, \tfrac{1}{2}\}\}.$$

We notice that $\mathcal{B}$ is a finite dimensional vector space of dimension N^2 which can be identified with X. Both $J(u) = \int_{\Omega_N} |Du|$ and $J_d^0(u)$ are norms on the quotient space $\mathcal{B}/\mathbb{R}$, hence they are equivalent. With a slight abuse of notation we shall indistinctly write $u \in \mathcal{B}$ or $u \in X$.

We shall assume that the convolution kernel $h \in L^2(\Omega_N)$ is such that $\hat{h}$ is supported in $\{-\frac{1}{2} + \frac{1}{N}, \dots, \frac{1}{2}\}$ and $\hat{h}(0,0) = 1$.

In the discrete framework, the ROF model for restoration is

$$\text{Minimize}_{u \in X} J_d^\beta(u) \tag{73}$$

$$\text{subject to} \quad \sum_{i,j=1}^{N} |(h * u)_{i,j} - f_{i,j}|^2 \le \sigma^2 N^2. \tag{74}$$

Notice again that the image acquisition model (1) is only incorporated through a global constraint. In practice, the above problem is solved via the following unconstrained formulation

$$\min_{u \in X} \max_{\alpha \ge 0} J_d^\beta(u) + \frac{\alpha}{2} \left[\frac{1}{N^2} \sum_{i,j=1}^{N} |(h * u)_{i,j} - f_{i,j}|^2 - \sigma^2 \right] \tag{75}$$

where $\alpha \ge 0$ is a Lagrange multiplier. The appropriate value of α can be computed using Uzawa's algorithm [3] so that the constraint (74) is satisfied. Recall that if we interpret α^{-1} as a penalization parameter which controls the importance of the regularization term, and we set this parameter to be small, then homogeneous zones are well denoised while highly textured regions will loose a great part of its structure. On the contrary, if α^{-1} is set to be small, texture will be kept but noise will remain in homogeneous regions. On the other hand, as the authors of [3] observed, if we use the constrained formulation (73)-(74) or, equivalently (75), then the Lagrange multiplier does not produce satisfactory results since we do not keep textures and denoise flat regions simultaneously, and they proposed to incorporate the image acquisition model as a set of local constraints.

Following [3], we propose to replace the constraint (74) by

$$G * (h * u - f)_{i,j} \le \sigma^2, \qquad \forall (i,j) \in \{1, \dots, N\}^2, \tag{76}$$

where G is a discrete convolution kernel such that $G_{i,j} > 0$ for all $(i,j) \in \{1,\dots,N\}^2$. The effective support of G must permit the statistical estimation of the variance of the noise with (76) [3]. Then we shall minimize the functional $J_d^\beta(u)$ on X submitted to the family of constraints (76) (plus eventually the constraint $\sum_{i,j=1}^N (h*u)_{i,j} = \sum_{i,j=1}^N f_{i,j}$). Thus, we propose to solve the optimization problem:

$$\begin{aligned} &\min_{u\in\mathcal{B}} J_d^\beta(u) \\ &\text{subject to } \; G*(h*u-f)_{i,j}^2 \le \sigma^2 \qquad \forall (i,j). \end{aligned} \tag{77}$$

This problem is well-posed, i.e., there exists a solution and is unique if $\beta > 0$ and $\inf_{c\in\mathbb{R}} G*(f-c)^2 > \sigma^2$. In case that $\beta = 0$ and $\inf_{c\in\mathbb{R}} G*(f-c)^2 > \sigma^2$, then $h*u$ is unique. Moreover, it can be solved with a gradient descent approach and Uzawa's method [3].

To guarantee that the assumptions of Uzawa's method hold we shall use a gradient descent strategy. For that, let $v \in X$ and $\gamma > 0$. At each step we have to solve a problem like

$$\begin{aligned} &\min_{u\in mathcalB} \gamma|u-v|_X^2 + J_d^\beta(u) \\ &\text{subject to } \; G*(h*u-f)_{i,j}^2 \le \sigma^2 \qquad \forall (i,j). \end{aligned} \tag{78}$$

We solve (78) using the unconstrained formulation

$$\min_{u\in X}\max_{\alpha\ge 0} \mathcal{L}^\gamma(u,\{\alpha\};v),$$

where $\alpha = (\alpha_{i,j})_{i,j=1}^N$ and

$$\mathcal{L}^\gamma(u,\{\alpha\};v) = \gamma|u-v|_X^2 + J_d^\beta(u) + \sum_{i,j=1}^N \alpha_{i,j}(G*(h*u-f)_{i,j}^2 - \sigma^2).$$

Algorithm: TV based restoration algorithm with local constraints

1. Set $u_0 = 0$ or, better, $u_0 = f$. Set $n = 0$.

2. Use Uzawa's algorithm to solve the problem

$$\min_{u\in X}\max_{\alpha\ge 0} \mathcal{L}^\gamma(u,\{\alpha\};u^n), \tag{79}$$

that is:

(a) Choose any set of values $\alpha_{i,j}^0 \ge 0$, $(i,j) \in \{1,\dots,N\}^2$, and $u_0^n = u^n$. Iterate from $p = 0$ until convergence of α^p the following steps:

(b) With the values of α^p solve DP(γ, u^n):

$$\min_u \mathcal{L}^\gamma(u,\{\alpha^p\};u^n)$$

starting with the initial condition u_p^n. Let u_{p+1}^n be the solution obtained.

(c) Update α in the following way:

$$\alpha_{i,j}^{p+1} = \max(\alpha_{i,j}^{p} + \rho(G * (h * u_p^n - f)_{i,j}^2 - \sigma^2), 0) \quad \forall (i,j).$$

Let u^{n+1} be the solution of (79). Stop when convergence of u^n.

We notice that, since $\gamma > 0$, Uzawa's algorithm converges if $f \in h * \mathcal{B}$. Moreover, if u^0 satisfies the constraints, then u^n tends to a solution u of (77) as $n \to \infty$ [3].

Finally, to solve problem (79) in Step 2.(b) of the Algorithm we use either the extension of Chambolle's algorithm [25] to the restoration case if we use $\beta = 0$, or the quasi-Newton method as in [4] adapted to solve (79) when $\beta > 0$. For more details, we refer to [3, 4] and references therein.

Figure 4: *Reference image and a filtered and noised image.* a) Left: reference image. b) Right: the data. This image has been generated applying the MTF given in (80) to the top image and adding a Gaussian white noise of zero mean and standard deviation $\sigma = 1$.

8.1 Some restoration experiments

To simulate our data we use the modulation transfer function corresponding to SPOT 5 HRG satellite with Hipermode sampling (see [55] for more details):

$$\hat{h}(\eta_1, \eta_2) = e^{-4\pi\beta_1|\eta_1|} e^{-4\pi\alpha\sqrt{\eta_1^2+\eta_2^2}} \mathrm{sinc}(2\eta_1)\mathrm{sinc}(2\eta_2)\mathrm{sinc}(\eta_1), \tag{80}$$

where $\eta_1, \eta_2 \in [-1/2, 1/2]$, $\mathrm{sinc}(\eta_1) = \sin(\pi\eta_1)/(\pi\eta_2)$, $\alpha = 0.58$, and $\beta_1 = 0.14$. Then we filter the reference image given in Figure 4.a with the filter (80) and we add some Gaussian white noise of zero mean and standard deviation σ (in our case $\sigma = 1$, which is a realistic assumption for the case of satellite images [55]) to obtain the image displayed in Figure 4.b.

Figure 5.a displays the restoration of the image in Figure 4.b obtained using the Algorithm of last section with $\beta = 0$. We have used a Gaussian function G of radius 6. The mean value

of the constraint is mean$((G*(Ku-f))^2) = 1.0933$ and RMSE $= 7.9862$. Figure 5.b displays the function $\alpha_{i,j}$ obtained.

Figure 6 displays some details of the results that are obtained using a single global constraint (74) and show its main drawbacks. Figure 6.a corresponds to the result obtained with the Lagrange multiplier $\alpha = 10$ (thus, the constraint (74) is satisfied). The result is not satisfactory because it is difficult to denoise smooth regions and keep the textures at the same time. Figure 6.b shows that most textures are lost when using a small value of α ($\alpha = 2$) and Figure 6.c shows that some noise is present if we use a larger value of α ($\alpha = 1000$). This result is to be compared with the same detail of Figure 5.a which is displayed in Figure 6.d.

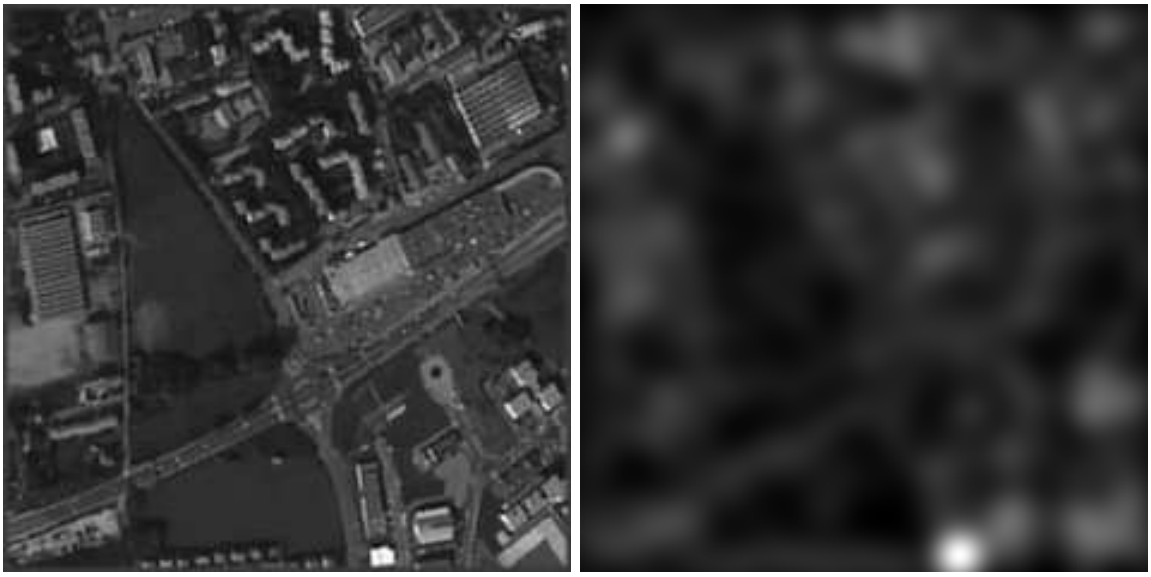

Figure 5: *Restored image with local Lagrange multipliers.* a) Left: the restored image corresponding to the data given in Figure 4.b. The restoration has been obtained using the Algorithm of last section with a Gaussian function G of radius 6. b) Right: the function $\alpha_{i,j}$ obtained.

8.2 The image model

For the purpose of image restoration the process of image formation can be modeled in a first approximation by the formula [55]

$$f = Q\big\{\Pi(h * u) + n\big\}, \tag{81}$$

where u represents the photonic flux, h is the point spread function of the optical-sensor joint apparatus, Π is a sampling operator, i.e. a Dirac comb supported by the centers of the matrix of digital sensors, n represents a random perturbation due to photonic or electronic noise, and Q is a uniform quantization operator mapping $\mathbb{R}$ to a discrete interval of values, typically $[0, 255]$.

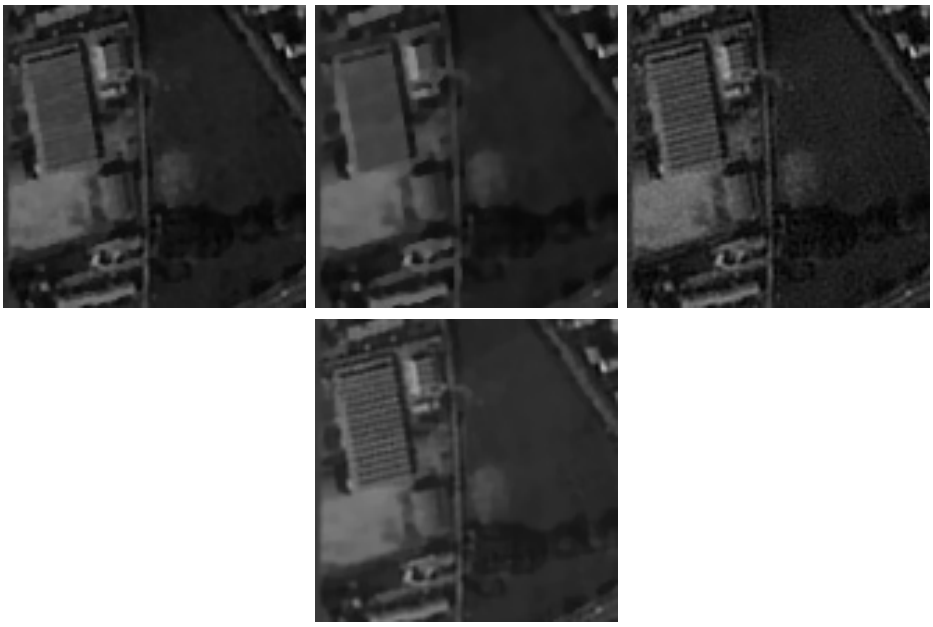

Figure 6: *A detail of the restored images with global and local constraints.* Top: a), b) and c) display a detail of the results that are obtained using a a single global constraint (74) and show its main drawbacks. Figure a) corresponds to the result obtained with the value of α such that the constraint (74) is satisfied, in our case $\alpha = 10$. Figure b) shows that most textures are lost when using a small value of α ($\alpha = 2$)and Figure c) shows that some noise is present if we use a larger value of α ($\alpha = 1000$). Bottom: d) displays the same detail of Figure 5.a which has been obtained using restoration with local constraints.

The modulation transfer function for satellite images. We describe here a simple model for the Modulation Transfer Function of a general satellite. More details can be found in [55] where specific examples of MTF for different acquisition systems are shown. The MTF used in our experiments (80) corresponds to a particular case of the general model described below [55].

Recall that the MTF, that we denote by $\hat{h}$, is the Fourier transform of the point spread function of the system. Let $(\eta_1, \eta_2) \in [-1/2, 1/2]$ denote the coordinates in the frequency domain. There are different parts in the acquisition system that contribute to the global transfer function: the optical system, the sensor, and the blur effects due to motion. Since each subsystem is considered as linear and translation invariant, it is modeled by a convolution operator. The kernel k of the joint system is thus the convolution of the point spread functions of the separated systems.

- Sensors: In CCD arrays every sensor has a sensitive region where all the photons that arrive are integrated. This region can be approximated by a unit square $[-c/2, c/2]^2$ where c is the distance between consecutive sensors. Its impulse response is then the convolution of two pulses, one in each spatial direction. The corresponding transfer function also includes the effect of the conductivity (diffusion of information) between neighbouring sensors, which

is modeled by an exponential decay factor, thus:

$$\hat{h}_S(\eta_1, \eta_2) = \text{sinc}(\eta_1 c)\text{sinc}(\eta_2 c)e^{-2\pi\beta_1 c|\eta_1|}e^{-2\pi\beta_2 c|\eta_2|},$$

where $\text{sinc}(\eta_1) = \sin(\pi\eta_1)/(\pi\eta_1)$ and $\beta_1, \beta_2 > 0$.

- Optical system: The optical system has essentially two effects on the image: it projects the objects from the object plane to the image plane and degrades it. The degradation of the image due to the optical system makes that a light point source looses definition and appears as a blurred (small) region. This effect can be explained by the wave nature of light and its diffraction theory. Discarding other degradation effects due to the imperfect optical systems like lens aberrations [12], the main source of degradation will be the diffraction of the light when passing through a finite aperture: those systems are called diffraction limited systems.

Assuming that the optical system is linear and translation invariant we know that it can be modeled by a convolution operator. Indeed, if the system is linear and translation invariant, it suffices to know the response of the system to a light point source located at the origin, which is modeled by a Dirac delta function δ, since any other light distribution could be approximated (in a weak topology) by superpositions of Dirac functions. The convolution kernel is, thus, the result of the system acting on δ.

If we measure the light intensity and we use a circular aperture the MTF is considered as an isotropic low-pass filter

$$\hat{h}_O(\eta_1, \eta_2) = e^{-2\pi\alpha c\sqrt{\eta_1^2+\eta_2^2}}, \quad \alpha > 0.$$

- Motion: each sensor counts the number of photons that arrive to its sensitive region during a certain time of acquisition. During the sampling time the system moves a distance τ and so does the sensor; this produces a motion blur effect in the motion direction (d_1, d_2):

$$\hat{h}_M(\eta_1, \eta_2) = \text{sinc}(\langle(\eta_1, \eta_2), (d_1, d_2)\rangle\tau).$$

Finally, the global MTF is the product of each of these intermediate transfer functions modeling the different aspects of the satellite:

$$\hat{h}(\eta_1, \eta_2) = \hat{h}_S\hat{h}_O\hat{h}_M.$$

Noise. We shall describe the typical noise in case of a CCD array. Light is constituted by photons (quanta of light) and those photons are counted by the detector. Typically, the sensor registers light intensity by transforming the number of photons which arrive to it into an electric charge, counting the electrons which the photons take out of the atoms. This is a process of a quantum nature and therefore there are random fluctuations in the number of photons and photoelectrons on the photoactive surface of the detector. To this source of noise we have to add the thermal fluctuations of the circuits that acquire and process the signal from the detector's photoactive surface. This random thermal noise is usually described by

a zero-mean white Gaussian process. The photoelectric fluctuations are more complex to describe: for low light levels, photoelectric emission is governed by Bose-Einstein statistics, which can be approximated by a Poisson distribution whose standard deviation is equal to the square root of the mean; for high light levels, the number of photoelectrons emitted (which follows a Poisson distribution) can be approximated by a Gaussian distribution which, being the limit of a Poisson process, inherits the relation between its standard deviation and its mean [12]. In a first approximation this noise is considered as spatially uncorrelated with a uniform power spectrum, thus a white noise. Finally, both sources of noise are assumed to be independent.

Taken together, both sources of noise are approximated by a gaussian white noise, which is represented in the basic equation (81) by the noise term n. The average signal to noise ratio, called the SNR, can be estimated by the quotient between the signals average and the square root of the variance of the signal.

The detailed description of the noise requires a knowledge of the precise system of image acquisition. More details in the case of satellite images can be found in [55] and references therein.

9 Final remarks: A different total variation based approach to denoising

Let us briefly comment on the interesting work [49] which interprets the total variation model for image denoising in a Bayesian way leading to a different algorithm based on stochastic optimization which produces better results.

We work again in the discrete setting and consider the image model

$$f_{i,j} = u_{i,j} + n_{i,j} \qquad (i,j) \in \{1,\dots,N\}^2, \tag{82}$$

where $n_{i,j}$ is a white Gaussian noise with zero mean and standard deviation σ.

The solution of (36) can be viewed as a Maximum a Posteriori (MAP) estimate of the original image u. Let $\beta > 0$ and let p_β be the prior probability density function defined by

$$p_\beta(u) \propto e^{-\beta J_d(u)} \qquad u \in X,$$

where we have omitted the normalization constant. The prior distribution models the gradient norms of each pixel as independent and identically distributed random variables following a Laplace distribution. Although the model does not exactly fit the reality since high gradient norms in real images are concentrated along curves and are not independent, it has been found to be convenient and efficient for many tasks in image processing and we follow it here.

Since the probability density of f given u is the density for $n = f - u$, then

$$p(f|u) \propto e^{-\frac{\|f-u\|_X^2}{2\sigma^2}}.$$

Figure 7: a) Left: the result obtained by computing $E(u|f)$ and $\beta\sigma^2 = \lambda = 20$, $\sigma = 10$ (image courtesy of Cécile Louchet). b) Right: the result obtained using Chambolle's algorithm with $\lambda = 20$.

Using Bayes rule, the posterior density of u given f is

$$p_\beta(u|f) = \frac{1}{Z} p(f|u) p_\beta(u) = \frac{1}{Z} e^{-\left(\frac{\|f-u\|_X^2}{2\sigma^2} + \beta J_d(u)\right)}, \tag{83}$$

where $Z = \displaystyle\int_{\mathbb{R}^{N^2}} e^{-\left(\frac{\|f-u\|_X^2}{2\sigma^2} + \beta J_d(u)\right)}\, du$ is the normalization constant making the mass of $p_\beta(u|f)$ to be 1. Then the maximization of the a posteriori density (83) is equivalent to the minimization problem (36) provided that $\beta\sigma^2 = \lambda$.

The estimation of u proposed in [49] consists in computing the expected value of u given f:

$$E(u|f) = \frac{1}{Z} \int_{\mathbb{R}^{N^2}} u p_\beta(u|f)\, du = \frac{1}{Z} \int_{\mathbb{R}^{N^2}} u e^{-\left(\frac{\|f-u\|_X^2}{2\sigma^2} + \beta J_d(u)\right)}\, du. \tag{84}$$

This estimate requires to compute an integral in a high dimensional space. In [49], the authors propose to approximate this integral with a Markov Chain Monte-Carlo algorithm (MCMC). In Figure 7.a we display the result of denoising the image in Figure 2.b which has a noise of standard deviation $\sigma = 10$ with the parameter $\beta = \frac{20}{\sigma^2}$. In Figure 7.b we display the denoising of the same image using Chambolle's algorithm with $\lambda = 20$. Notice that in both cases the parameter λ is the same.

Acknowledgement. We would like to thank Cécile Louchet for providing us the experiments of Section 9, and Gabriele Facciolo and Enric Meinhardt for the experiements in Section 7.1. V. Caselles acknowledges partial support by PNPGC project, reference MTM2006-14836 and also by "ICREA Acadèmia" for excellence in research funded by the Generalitat de Catalunya.

References

[1] R. K. Ahuja, T. L. Magnanti, and J. B. Orlin. Network flows. Theory, algorithms, and applications. Prentice Hall Inc., Englewood Cliffs, NJ, 1993.

[2] W. K. Allard. Total Variation regularization for image denoising: I. Geometric theory. *Siam J. Math. Anal.* (to appear), 2008. Total Variation regularization for image denoising: II. Examples. *SIAM Journal on Imaging Sciences* (to appear), 2009

[3] A. Almansa, C. Ballester, V. Caselles, and G. Haro. A TV based restoration model with local constraints. *J. Sci. Comput.* **34**, 209–236, 2008.

[4] A. Almansa, J.F. Aujol, V. Caselles, and G. Facciolo. Irregular to regular sampling, denoising and deconvolution. *SIAM J. Mult. Model. Simul.* (to appear), 2009.

[5] F. Alter and V. Caselles. Uniqueness of the Cheeger set of a convex body. *Nonlinear Analysis, TMA* **70**, 32-44, 2009.

[6] F. Alter, V. Caselles, and A. Chambolle. Evolution of Convex Sets in the Plane by the Minimizing Total Variation Flow. *Interfaces and Free Boundaries* **7**, 29-53, 2005.

[7] F. Alter, V. Caselles, and A. Chambolle. A characterization of convex calibrable sets in $\mathbb{R}^N$. *Math. Ann.* **332**, 329-366, 2005.

[8] M. Amar and G. Bellettini. A notion of total variation depending on a metric with discontinuous coefficients. *Ann. Inst. Henri Poincaré* **11**, 91–133, 1994.

[9] L. Ambrosio. Corso introduttivo alla teoria geometrica della misura ed alle superfici minime. Scuola Normale Superiore, Pisa, 1997.

[10] L. Ambrosio, N. Fusco, and D. Pallara. Functions of Bounded Variation and Free Discontinuity Problems. Oxford Mathematical Monographs, 2000.

[11] F. Andreu, V. Caselles, and J.M. Mazón. Parabolic Quasilinear Equations Minimizing Linear Growth Functionals. Progress in Mathematics 223, Birkhauser Verlag, 2004.

[12] H.C. Andrews and B.R. Hunt. Digital Signal Processing. Tech. Englewood Cliffs, NJ, Prentice Hall, 1977.

[13] A. Beck and M. Teboulle. A fast iterative shrinkage-thresholding algorithm for linear inverse problems. *to appear*, 2008.

[14] G. Bellettini, V. Caselles, and M. Novaga. The Total Variation Flow in $\mathbb{R}^N$. *J. Differential Equations* **184**, 475-525, 2002.

[15] G. Bellettini, V. Caselles, and M. Novaga, Explicit solutions of the eigenvalue problem $-\mathrm{div}\left(\frac{Du}{|Du|}\right) = u$ in $\mathbb{R}^2$. *SIAM Journal on Mathematical Analysis* **36**, 1095–1129, 2005.

[16] Y. Boykov and V. Kolmogorov. An experimental comparison of min-cut/max-flow algorithms for energy minimization in vision. *IEEE Trans. Pattern Analysis and Machine Intelligence* **26**(9), 1124–1137, 2004.

[17] A. Buades, B. Coll, and J.M. Morel. A non local algorithm for image denoising. In *Proc. of the IEEE Conf. on CVPR*, volume 2, pp. 60–65, 2005.

[18] V. Caselles, A. Chambolle, and M. Novaga. Uniqueness of the Cheeger set of a convex body. *Pacific Journal of Mathematics* **232**, 77-90, 2007.

[19] V. Caselles and A. Chambolle. Anisotropic curvature-driven flow of convex sets. *Nonlinear Analysis, TMA.* **65** , 1547-1577, 2006.

[20] V. Caselles, A. Chambolle, and M. Novaga. The discontinuity set of solutions of the TV denoising problem and some extensions. *SIAM Mult. Model. Simul.* **6**, 879–894, 2007.

[21] V. Caselles, A. Chambolle, and M. Novaga. Regularity for solutions of the Total Variation denoising problem. Preprint, 2009.

[22] V. Caselles, G. Facciolo, and E. Meinhardt. Anisotropic Cheeger sets and applications. Preprint, 2008.

[23] V. Caselles, R. Kimmel, and G. Sapiro. Geodesic Active Contours, *Inter. Journal Computer Vision* **22**(1), 61-79, 1997.

[24] A. Chambolle and P.L. Lions. Image Recovery via Total Variation Minimization and Related Problems. *Numer. Math.* **76**, 167-188, 1997.

[25] A. Chambolle. An algorithm for total variation minimization and applications. *Journal of Mathematical Imaging and Vision* **20**, 89-97, 2004.

[26] A. Chambolle. An algorithm for mean curvature motion. *Interfaces and Free Boundaries* **6**, 195-218, 2004.

[27] A. Chambolle. Total variation minimization and a class of binary MRF models. In *Energy Minimization Methods in Computer Vision and Pattern Recognition*, Lecture Notes in Computer Science, pages 136–152, 2005.

[28] A. Chambolle and J. Darbon. On Total variation minimization and Surface Evolution using Parametric Maximum Flows, Preprint, 2009.

[29] A. Chambolle, D. Cremers, and T.Pock. A convex approach for computing minimal partitions. Peprint R.I. 649, CMA Ecole Polytechnique, 2008.

[30] T. F. Chan, G.H. Golub, and P. Mulet. A Nonlinear Primal-Dual Method for Total Variation Based Image Restoration. *SIAM J. Sci. Comput.* **20**, 1964-1977, 1999.

[31] T.F. Chan, S. Esedoglu, and M. Nikolova. Algorithms for finding global minimizers of image segmentation and denoising methods. *SIAM J. Appl. Math.* **66**, 1632–1648, 2006.

[32] T.F. Chan and L.A. Vese. Active contours without edges. *IEEE Transactions on Image Processing* **10**(2), 266-277, 2001.

[33] J. Darbon and M. Sigelle. Image restoration with discrete constrained Total Variation part I: Fast and exact optimization. *Journal of Mathematical Imaging and Vision* **26**(3), 261–276, 2006.

[34] E. De Giorgi and L. Ambrosio. Un nuovo tipo di funzionale del calcolo delle variazioni. *Atti Accad. Naz. Lincei Rend. Cl. Sci. Mat Fis. Natur. s. 8* **82**, 199-210, 1988.

[35] E. De Giorgi, M. Carriero, and A. Leaci. Existence theorem for a minimum problem with free discontinuity set. *Arch. Rational Mech. Anal.* **108**(3), 195-218, 1989.

[36] G. Demoment. Image reconstruction and restoration: Overview of common estimation structures and problems. *IEEE Transactions on Acoustics, Speech and Signal Processing* **37**(12), 2024-2036, 1989.

[37] S. Durand, F. Malgouyres, and B. Rougé. Image Deblurring, Spectrum Interpolation and Application to Satellite Imaging. *ESAIM Control Optim. Calc. Var.* **5**, 445-475, 2000.

[38] M. J. Eisner and D. G. Severance. Mathematical techniques for efficient record segmentation in large shared databases. *J. Assoc. Comput. Mach.* **23**(4), 619–635, 1976.

[39] E. Esser, X. Zhang, and T. Chan. A general framework for a class of first order primal-dual algorithms for tv minimization. CAM Reports 09-67, UCLA, Center for Applied Math., 2009.

[40] G. Gallo, M. D. Grigoriadis, and R. E. Tarjan. A fast parametric maximum flow algorithm and applications. *SIAM J. Comput.* **18**, 30–55, 1989.

[41] D. Goldfarb and Y. Yin. Parametric maximum flow algorithms for fast total variation minimization. Technical report, Rice University, 2007.

[42] Y. Gousseau and J.M. Morel. Are natural images of bounded variation? *SIAM J. Math. Anal.* **33**, 634-648, 2001.

[43] D. M. Greig, B. T. Porteous, and A. H. Seheult. Exact maximum a posteriori estimation for binary images. *J. R. Statist. Soc. B* **51**, 271–279, 1989.

[44] D. S. Hochbaum. An efficient algorithm for image segmentation, Markov random fields and related problems. *J. ACM* **48**(4), 686–701 (electronic), 2001.

[45] S. Kichenassamy, A. Kumar, P. Olver, A. Tannenbaum, and A. Yezzi. Conformal curvature flows: from phase transitions to active vision. *Arch. Rat.Mech. Anal.* **134**, 275-301, 1996.

[46] V. Kolmogorov, Y. Boykov, and C. Rother. Applications of parametric maxflow in computer vision. In *Proceedings of the IEEE 11th International Conference on Computer Vision (ICCV 2007)*, pp. 1–8, 2007.

[47] V. Kolmogorov and R. Zabih. What energy functions can be minimized via graph cuts? *IEEE Trans. Pattern Analysis and Machine Intelligence* **2**(26), 147–159, 2004.

[48] N. Korevaar. Capillary surface convexity above convex domains. *Indiana Univ. Math. J.* **32**, 73-82, 1983.

[49] C. Louchet and L. Moisan. Total Variation denoising using posterior expectation. In *Proc. of the European Signal Proc. Conf. (EUSIPCO), Lausanne*, August 2008.

[50] Y. Meyer. Oscillating patterns in image processing and nonlinear evolution equations. The fifteenth Dean Jacqueline B. Lewis memorial lectures. University Lecture Series, 22. American Mathematical Society, Providence, RI, 2001.

[51] Y. Nesterov. Smooth minimization of nonsmooth functions. *Mathematical programming Series A*, **103**, 127–152, 2005.

[52] M. Nikolova. Local strong homogeneity of a regularized estimator. *SIAM J. Appl. Math.* **61**, 633–658, 2000.

[53] J. C. Picard and H. D. Ratliff. Minimum cuts and related problems. *Networks* **5**(4), 357–370, 1975.

[54] T. Pock, T. Schoenemann, D. Cremers, and H. Bischof. A convex formulation of continuous multi-label problems. In *European Conference on Computer Vision (ECCV), Marseille, France,* October 2008.

[55] B. Rougé. Théorie de l'echantillonage et satellites d'observation de la terre. *Analyse de Fourier et traitement d'images*, Journées X-UPS 1998.

[56] L. Rudin and S. Osher. Total Variation based Image Restoration with Free Local Constraints. In *Proc. of the IEEE ICIP-94*, vol. 1, Austin, TX, pp. 31-35, 1994.

[57] L. Rudin, S. Osher, and E. Fatemi. Nonlinear Total Variation based Noise Removal Algorithms. *Physica D.* **60**, 259-268, 1992.

[58] O. Scherzer, M. Grasmair, H. Grossauer, M. Haltmeier, and F. Lenzen. Variational methods in imaging. Applied Mathmatical Sciences, Spriner Verlag, 2008.

[59] L. Vese. A Study in the BV Space of a Denoising-Deblurring Variational Problem. *Appl. Math. Optim.* **44**, 131-161, 2001.

[60] M. Zhu and T.F. Chan. An efficient primal-dual hybrid gradient algorithm for total variation image restoration. Preprint 2008.

[61] W. P. Ziemer. *Weakly Differentiable Functions*, GTM 120, Springer Verlag, 1989.